Article

Cell Reports

TET2 Regulates the Neuroinflammatory Response in Microglia

Graphical Abstract

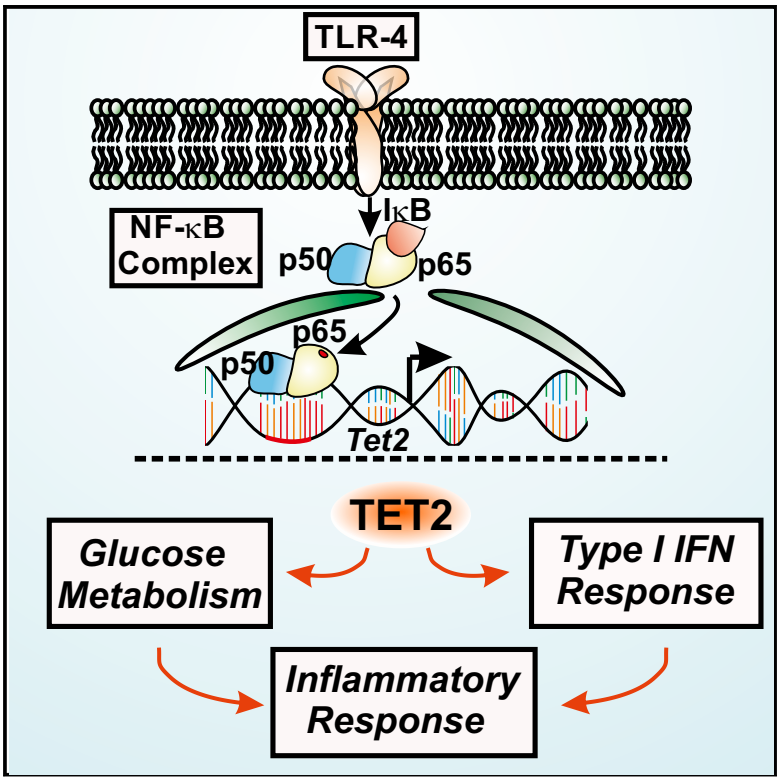

Authors

Alejandro Carrillo-Jimenez, Özgen Deniz, Maria Victoria Niklison-Chirou, ..., Jose Luis Venero, Miguel Ramos Branco, Miguel Angel Burguillos

Correspondence

m.branco@qmul.ac.uk (M.R.B.), maburguillos@us.es (M.A.B.)

In Brief

Microglia play a key role in neuroinflammation and neurodegeneration in different neurodegenerative diseases, but little is known about the epigenetic modifying enzymes regulating their inflammatory response. Carrillo-Jimenez et al. identify TET2 as a major regulator of the microglia proinflammatory response and suggest that, by targeting this protein, microglial activation could be impaired.

Highlights

- TET2 is upregulated in microglia cells upon various inflammatory stimuli
- TET2 regulates TLR-4-induced type I IFN response and LPS-induced aerobic glycolysis
- TET2 regulates the proinflammatory response induced by LPS *in vitro* and *in vivo*
- TET2 is expressed by amyloid β plaque-associated microglia in AD brains

Carrillo-Jimenez et al., 2019, Cell Reports *29*, 697–713
October 15, 2019
https://doi.org/10.1016/j.celrep.2019.09.013

CellPress

Cell Reports
Article

TET2 Regulates the Neuroinflammatory Response in Microglia

Alejandro Carrillo-Jimenez,[1,2,9] Özgen Deniz,[3,9] Maria Victoria Niklison-Chirou,[3,9] Rocio Ruiz,[1,2,9] Karina Bezerra-Salomão,[3,11] Vassilis Stratoulias,[4] Rachel Amouroux,[5] Ping Kei Yip,[3] Anna Vilalta,[6] Mathilde Cheray,[4] Alexander Michael Scott-Egerton,[3] Eloy Rivas,[7] Khadija Tayara,[1,2] Irene García-Domínguez,[1,2] Juan Garcia-Revilla,[1,2] Juan Carlos Fernandez-Martin,[1,2] Ana Maria Espinosa-Oliva,[1,2] Xianli Shen,[4] Peter St George-Hyslop,[8] Guy Charles Brown,[6] Petra Hajkova,[5] Bertrand Joseph,[4] Jose Luis Venero,[1,2,10] Miguel Ramos Branco,[3,10,*] and Miguel Angel Burguillos[1,2,3,10,12,*]

[1]Instituto de Biomedicina de Sevilla (IBiS), Hospital Universitario Virgen del Rocío/CSIC/Universidad de Sevilla, 41013 Sevilla, Spain
[2]Departamento de Bioquímica y Biología Molecular, Facultad de Farmacia, Universidad de Sevilla, 41012 Sevilla, Spain
[3]Blizard Institute, Barts and The London School of Medicine and Dentistry, QMUL, London E1 2AT, UK
[4]Institute of Environmental Medicine, Toxicology Unit, Karolinska Institutet, 171 77 Stockholm, Sweden
[5]MRC London Institute of Medical Sciences/Institute of Clinical Sciences Faculty of Medicine, Imperial College London, Du Cane Road, London W12 0NN, UK
[6]Department of Biochemistry, University of Cambridge, Tennis Court Road, Cambridge CB2 1QW, UK
[7]Department of Pathology, Instituto de Biomedicina de Sevilla, Hospital Universitario Virgen del Rocío/CSIC/Universidad de Sevilla, 41013 Sevilla, Spain
[8]Department of Clinical Neurosciences, Cambridge Institute for Medical Research, University of Cambridge, Cambridge CB2 0SP, UK
[9]These authors contributed equally
[10]Senior author
[11]Present address: Department of Genetics, Ribeirão Preto School of Medicine, University of São Paulo, 3900 Bandeirantes Avenue, 14049-900 Ribeirão Preto, SP, Brazil
[12]Lead Contact
*Correspondence: m.branco@qmul.ac.uk (M.R.B.), maburguillos@us.es (M.A.B.)
https://doi.org/10.1016/j.celrep.2019.09.013

SUMMARY

Epigenomic mechanisms regulate distinct aspects of the inflammatory response in immune cells. Despite the central role for microglia in neuroinflammation and neurodegeneration, little is known about their epigenomic regulation of the inflammatory response. Here, we show that Ten-eleven translocation 2 (TET2) methylcytosine dioxygenase expression is increased in microglia upon stimulation with various inflammogens through a NF-κB-dependent pathway. We found that TET2 regulates early gene transcriptional changes, leading to early metabolic alterations, as well as a later inflammatory response independently of its enzymatic activity. We further show that TET2 regulates the proinflammatory response in microglia of mice intraperitoneally injected with LPS. We observed that microglia associated with amyloid β plaques expressed TET2 in brain tissue from individuals with Alzheimer's disease (AD) and in 5xFAD mice. Collectively, our findings show that TET2 plays an important role in the microglial inflammatory response and suggest TET2 as a potential target to combat neurodegenerative brain disorders.

INTRODUCTION

Microglia, the resident immune cells in the CNS, are key players in maintaining homeostasis in the brain. Microglia play a wide variety of roles under physiological and pathological conditions. In the healthy brain, microglia are responsible for neuronal activity-dependent synapse pruning during postnatal development (Schafer et al., 2012; Wu et al., 2015). Upon neuronal injury or infection, microglia become rapid responders that initiate an innate inflammatory response (Hanisch and Kettenmann, 2007). If the inflammatory response is exaggerated or chronic, it becomes detrimental for the surrounding neuronal population, as in Parkinson's disease (PD) and Alzheimer's diseases (AD) (Burguillos et al., 2011; Perry and Holmes, 2014; Abeliovich and Gitler, 2016; Ransohoff, 2016), as well as ischemic stroke (Lambertsen et al., 2012; Burguillos et al., 2015).

In PD or AD, only a minor subset of patients carry genetic mutations contributing to disease development (Pickrell and Youle, 2015; Abeliovich and Gitler, 2016; Van Cauwenberghe et al., 2016). Most cases appear to be a combination of genetic predisposition and exposure to environmental risk factors. The identification of mutations in innate immunity-related genes that confer higher risk for developing neurodegenerative diseases supports the idea of microglia playing a key role in driving disease pathogenesis (Malik et al., 2015). Hence, epigenetic mechanisms are prime candidates for mediating environmentally driven alterations to immune homeostasis. Indeed, the contribution of epigenetic modifications in PD (Park et al., 2016; Wüllner

et al., 2016) and AD (Phipps et al., 2016; Watson et al., 2016), has been addressed in a number of studies. However, despite the key role of microglia in the neuroinflammatory response in those neurodegenerative diseases, little is known about the epigenetic regulation of the inflammatory response in these cells.

Major epigenetic mechanisms include post-translational modification of histones, DNA methylation at CpG dinucleotides, and regulation by non-coding RNAs (Bonasio et al., 2010). Interestingly, the age-dependent increase in microglial IL-1β levels is associated with DNA hypomethylation within the *IL-1β* promoter (Matt et al., 2016), which is seemingly driven by the age-dependent loss of SIRT1 (a NAD-dependent deacetylase) (Cho et al., 2015). DNA methylation could therefore play key roles in regulating the inflammatory state in microglia. Importantly, DNA methylation can be removed by the action of Ten-eleven translocation (TET) enzymes, which are dioxygenases that catalyze the oxidation of 5-methylcytosine (5mC) into 5-hydroxymethylcytosine (5hmC) and other oxidative derivatives (Branco et al., 2011). Recently, TETs have been shown to play various roles in the physiology of immune cells, including thymocytes (Tsagaratou et al., 2017), T helper cells (Ichiyama et al., 2015), dendritic cells (Zhang et al., 2015), and bone marrow-derived macrophages (Zhang et al., 2015; Cull et al., 2017).

Here, we investigated the role of TET enzymes in the inflammatory response in microglia cells upon Toll-like receptor 4 (TLR-4) activation. We found that TET2 regulates both early transcription (after only a few hours) of genes affecting several pathways (including control of the immune response and cell cycle) and the late inflammatory response. We confirmed *in vivo* that TET2 regulates the proinflammatory response in microglia cells. Furthermore, we show that TET2 is expressed in microglia close to amyloid β (Aβ) plaques in both human AD subjects and in 5xFAD mice. All these results highlight the potential of TET2 as a novel drug target for neurodegenerative diseases, including AD.

RESULTS

TLR Activation in Microglia Induces Upregulation of Tet2 Expression

To assess the effect of TLR-4 activation on the expression of TET enzymes in microglia, we treated the murine BV2 microglial cell line with LPS. We found that LPS (1 μg/mL) induced both an early 2 h (Figure 1A) and sustained 24 h (Figure 1B) upregulation of *Tet2* expression. However, the expression of the other two members of the TET family (TET1 and TET3) either did not vary upon LPS treatment (*Tet3*; Figure 1A) or was not detectable (*Tet1*; not shown) before or after LPS treatment. In concordance with the RNA data, we detected an increase of TET2 expression at the protein level 6 h after LPS treatment (Figure 1C). Interestingly, a lower dose of LPS (0.1 μg/mL) also induced *Tet2* expression as early as 2 h after treatment (Figure 1D). To rule out the possibility that LPS-induced TET2 expression might be due to the transformed origin of our murine microglia cell line (Butovsky et al., 2014), we analyzed the expression of *Tet2* in primary adult and postnatal primary microglia cells from mouse and rat origin 6 h after LPS treatment and obtained similar results to those seen in BV2 microglia cells (Figure 1E). Notably, we also observed a mild but significant upregulation of *TET2* in human microglia cells (CHME3 human microglia cell line) (Figure 1E). We further validated our observations by analyzing RNA sequencing (RNA-seq) data from postnatal primary microglia cell culture experiments (Janova et al., 2016), which showed that *Tet2* expression was increased both at low and high levels of LPS treatment, as well as after treatment with fibronectin, which also promotes inflammation (Figure S1A). Fibronectin-mediated regulation of *Tet2* suggests that *Tet2* upregulation might not only be driven by TLR-4 activation. For this reason, we challenged our BV2 cells with lipoteichoic acid (LTA), a known TLR-2 ligand, and observed a similar pattern in the expression of *Tet2* and *Tet3* to that seen in LPS-treated cells (Figures S1B and S1C). These data show that multiple TLR agonists drive *Tet2* upregulation in microglia from different species.

NF-κB p65 Mediates LPS-Induced Tet2 Expression

We then sought to investigate the mechanisms responsible for the transcriptional regulation of *Tet2* upon TLR-4 activation. We first took advantage of published chromatin immunoprecipitation sequencing (ChIP-seq) data on the TLR-4-induced "enhancer landscape" in macrophages (Kaikkonen et al., 2013). We used these data as a model for TLR-4-induced regulatory events that may also be occurring in microglia cells. We mapped data for the activating histone mark H3K27ac, as well as various transcription factors, and visually inspected the promoter and upstream regions of *Tet2* (profiles in Figure 2A and Figure S2A). In untreated macrophages, H3K27ac was enriched both at the promoter region of *Tet2* and a region lying 40 kb upstream, thus constituting a putative distal enhancer element (Figure 2A). Notably, the levels of H3K27ac increased in the upstream region (E1 and E2) after 1 h treatment with Kdo2-lipid A (KLA) (a TLR-4 agonist), and this was concomitant with the recruitment of p65 to both the promoter and upstream regions upon KLA treatment (Figure 2C). In contrast, the binding of CEBPA and PU.1 was largely unaffected by KLA treatment (Figure S2A), suggesting that p65 is a major driver of TLR-4-dependent activation of *Tet2*. To test whether similar patterns can be observed in BV2 cells, we performed ChIP followed by qPCR analysis at the promoter and upstream regions of *Tet2*. In concordance with the results obtained from bone marrow-derived macrophages (Figure 2A), BV2 cells are enriched for H3K27ac at the *Tet2* promoter and at the putative regulatory region upstream of *Tet2* (Figure 2B). Interestingly, H3K27ac levels specifically increased in the upstream region upon LPS treatment (Figure 2B). Moreover, we detected enrichment for H3K4me1, a histone mark associated with both poised and active enhancer elements, providing support for the upstream region being an enhancer element that becomes active upon TLR-4 activation (Creyghton et al., 2010). We then analyzed p65 enrichment in the promoter and enhancer regions of *Tet2* upon LPS treatment in BV2 cells and observed a clear increase in p65 binding at the enhancer region, whereas LPS more subtly modulated the binding of p65 at the promoter region (Figure 2D). We analyzed the promoter regions of NF-κB inhibitor alpha (*NFκBia*) and *Il-1β* as positive controls for LPS-dependent p65 binding (Figure S2B). These results suggest a

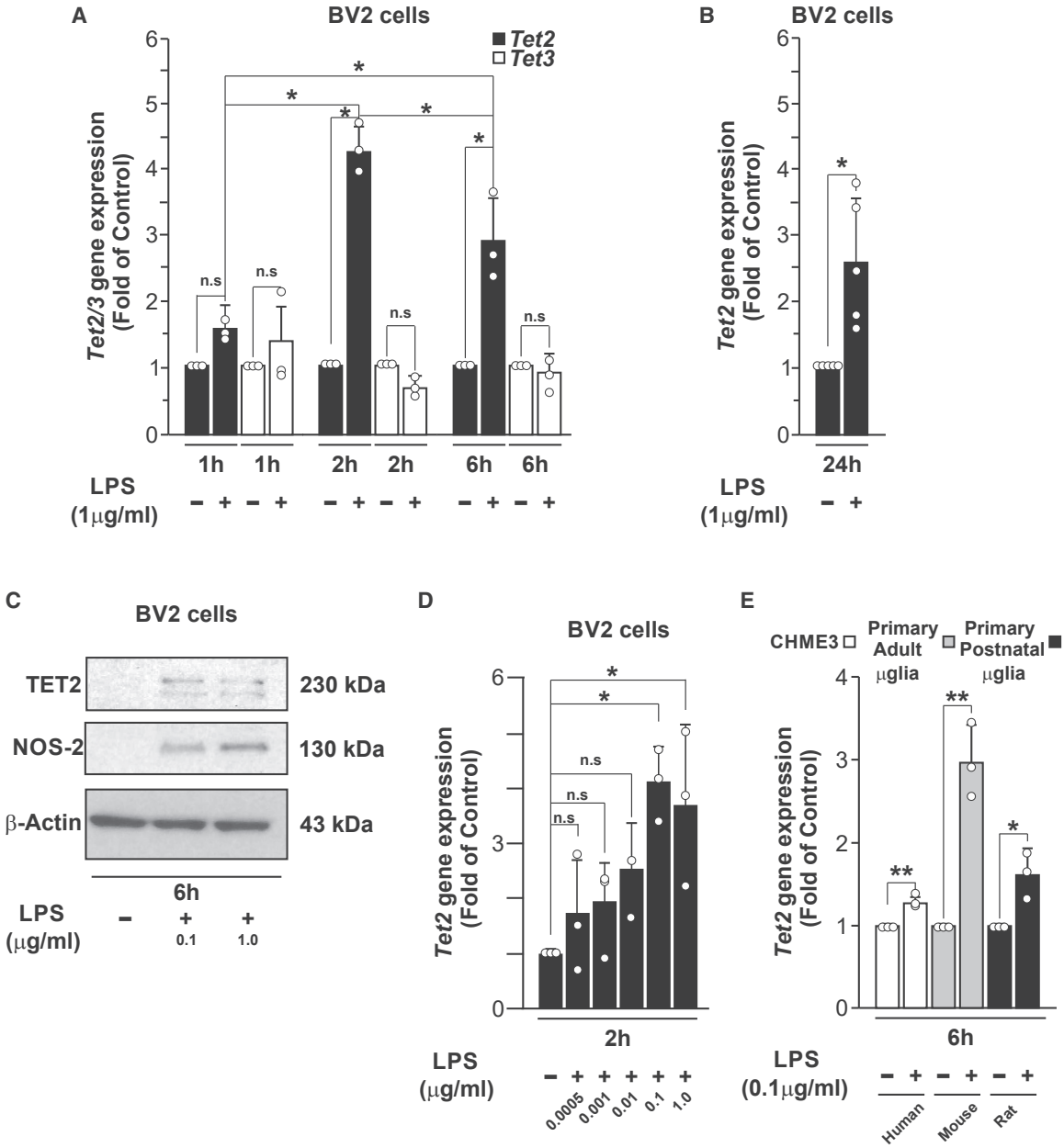

Figure 1. LPS Induces an Early and Sustained Expression of *Tet2* in Microglia Cells

(A and B) *Tet2* and *Tet3* expression in BV2 microglia cells treated with LPS (1 μg/mL) at 1, 2 and 6 h (A) and *Tet2* expression after 24 h treatment with LPS (1 μg/mL) (B).

(C) Representative immunoblot showing increase of TET2 and NOS-2 expression (a positive control of microglia activation) at 6 h after LPS treatment (0.1 and 1 μg/mL) in BV2 cells.

(D) *Tet2* LPS-induced dose-response in BV2 microglial cells at 2 h.

(E) *Tet2* gene expression after 6 h LPS (0.1 μg/mL) treatment in human microglial cell line (CHME3), primary adult microglia in mouse, and primary postnatal microglia culture in rat.

Statistical analysis was performed using one-way ANOVA with Scheffé (A and B) and LSD (D) corrections or two-tailed Student's t test (E). Data shown are mean ± SD of three (A, D, and E) and five (B) independent experiments. *$p < 0.05$ and **$p < 0.01$.

See also Figure S1.

potential role of p65 in*Tet2* expression through binding to an upstream enhancer element, increasing its activity, which is reflected by the higher H3K27ac levels in LPS-treated cells.

To test the functional relevance of increased p65 binding to the upstream region of *Tet2* in regulating *Tet2* expression upon LPS treatment, we pre-treated BV2 cells for 1 h with wedelolactone,

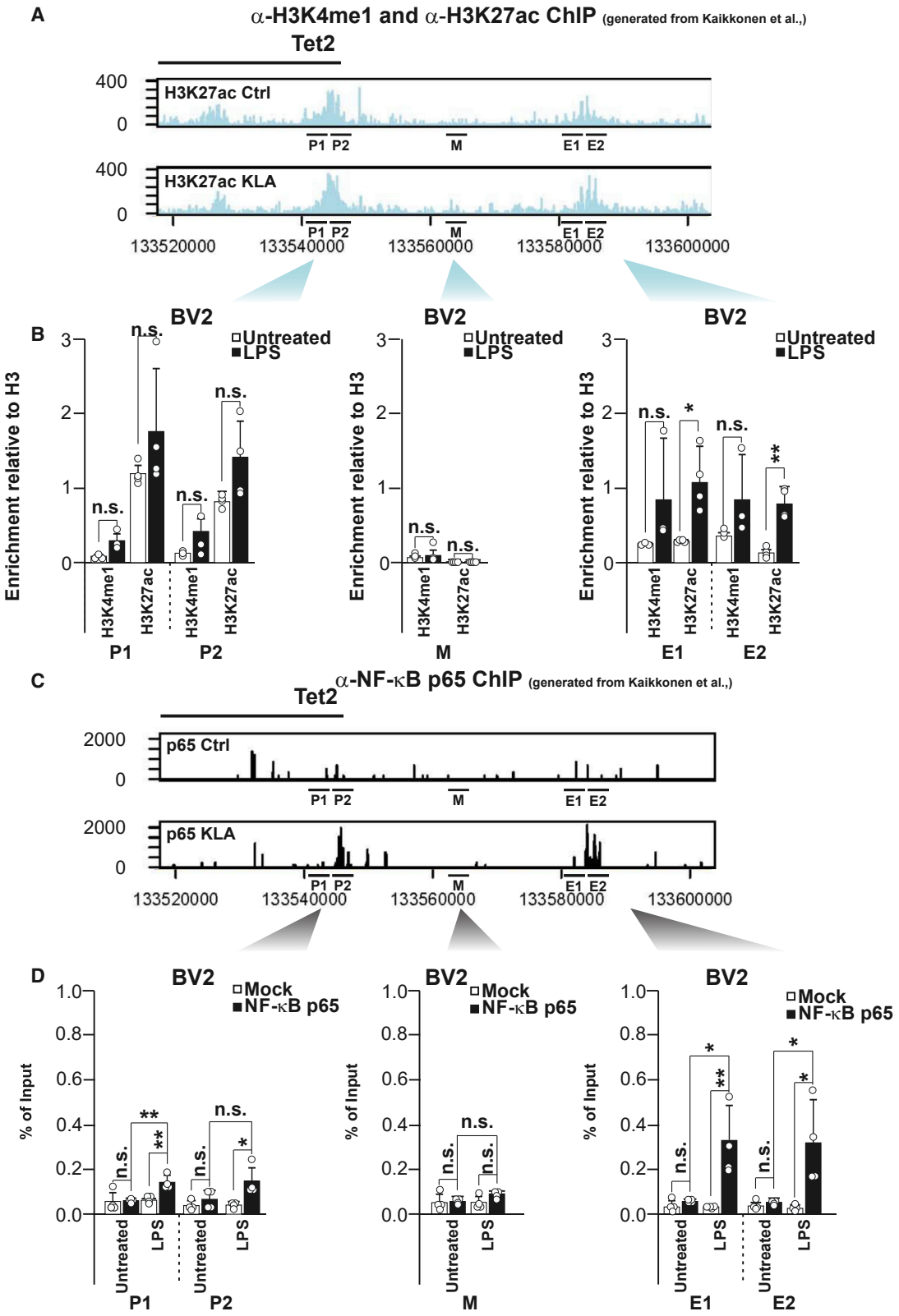

(legend on next page)

an inhibitor of the IKK complex, followed by treatment with LPS for 6 h. We used *Il-1β* as a positive control, as its transcription has been shown to be regulated by NF-κB (Cogswell et al., 1994) (Figure S2C). In line with our ChIP-qPCR data, LPS-induced expression of *Tet2* was abrogated in the presence of wedelolactone (Figure S2D), suggesting that the NF-κB complex plays a role in regulating *Tet2* expression (either directly or indirectly) upon LPS treatment.

TET2 Helps Drive the Expression of Genes Induced by TLR-4 Stimulation

Given the reported involvement of TET2 in the regulation of immune functions, we asked whether it also plays a role during the neuroinflammatory response. For this purpose, we depleted *Tet2* in BV2 microglia cells using a small interfering RNA (siRNA; siTET2) strategy prior to LPS treatment (Figure 3A). To confirm that TET2 depletion resulted in decreased enzymatic activity, we measured global 5hmC levels using mass spectrometry and observed a significant 5hmC reduction in *Tet2*-knockdown cells compared with a non-targeting control (Figure 3B). Interestingly, LPS treatment did not change global 5hmC levels, despite the increase in TET2 expression. We then performed RNA-seq on TET2-depleted cells, before and after 3 h of LPS treatment, and compared them against a non-targeting control. First, we checked that the expression pattern in our BV2 cells after LPS treatment is very similar to previously published RNA-seq data from LPS-treated primary microglia cells in (Janova et al., 2016) (Figure S3A). To identify genes whose activation or repression during LPS treatment depends on TET2, we intersected LPS-regulated genes with TET2-regulated ones. Of 1,565 genes that were upregulated by LPS, 140 (9%) had reduced expression in TET2-depleted cells (Figure S3B). Conversely, of 1,110 genes repressed by LPS, 38 (3%) had increased expression in TET2-depleted cells (Figure S3B). Both groups of TET2-regulated genes displayed an impaired response to LPS in *Tet2*-knockdown cells, as judged by significant differences in the expression fold change upon LPS treatment (Figure 3C). We validated several of the gene expression changes mediated by TET2 depletion in LPS-treated cells (Figure S3C) by qPCR. Gene Ontology analyses revealed that the 140 siTET2-downregulated genes are associated mainly with the control of the innate immune response, including the response to interferon (IFN)-β (or type I IFN response), whereas the 38 siTET2-upregulated genes are associated with cell cycle regulation (Figure 3D). A manual classification of gene function on the basis of literature searches confirmed an enrichment for inflammatory and cell cycle-related genes in TET2-regulated targets, followed by genes related to intracellular signaling and transcription factors (Figure 3E). Interestingly, Gene Ontology analysis on siTET2-downregulated genes that are not modified by LPS treatment revealed a similar enrichment for genes involved in the immune response (Figure 3F). This result suggests that the effect of TET2 over the inflammatory response is not unique to LPS treatment but can also potentially affect other immune signaling pathways.

To rule out the possibility that the observed gene deregulation was due to increased cell death, we performed fluorescence-activated cell sorting (FACS) analyses of control and TET2-depleted cells. We could not find any indication of induction of cell death (Figures S3D–S3G) or major change in morphology (Figure S3H), suggesting a direct effect of TET2 over many of those genes upon treatment.

TET2 Does Not Affect DNA Methylation Levels at Target Genes

TET2 has been shown to act via both 5mC oxidation and catalytic-independent mechanisms, such as recruitment of epigenetic modifiers (Ichiyama et al., 2015; Zhang et al., 2015). Therefore, we investigated whether the regulatory effect of TET2 on LPS-driven gene expression in microglia was dependent on its catalytic activity. We first analyzed global 5mC levels by mass spectrometry in LPS-treated cells, comparing TET2-depleted cells with controls (Figure S4A). Neither LPS treatment nor knockdown of TET2 resulted in a significant change in global 5mC levels (Figure S4A), despite the fact that global 5hmC levels were altered in siTET2 cells (Figure 3B). In order to determine whether TET2-mediated 5mC oxidation occurs in a locus-specific manner, we used oxidative bisulfite sequencing (oxBS-seq) (de la Rica et al., 2016; Booth et al., 2012) and measured 5mC and 5hmC levels at the promoters of six target genes whose expression levels were altered by TET2 knockdown (Figures 4A–4F; Figures S4B–S4G). No significant changes were detected in the levels of 5mC (Figures 4A–4F). In 5hmC levels, we observed some statistically significant but very minor differences (Figure S4C). These results suggest that the action of TET2 on these genes does not involve its catalytic activity at these gene promoters. In line with this, our mass spectrometry data show that LPS treatment does not induce global changes in 5hmC levels, suggesting that increased TET2 catalytic activity is not necessary to mediate gene expression changes upon LPS treatment.

The effect of TET2 on the expression of selected genes could also be explained by indirect effects. To test whether TET2 was bound to the promoters of genes affected by TET2 depletion, we

Figure 2. NF-κBp65 Regulates LPS-Induced *Tet2* Transcription

(A) Profile of H3K27ac marking at the *Tet2* promoter and upstream regions after 1 h treatment of macrophages with KLA, generated from published ChIP-seq data (Kaikkonen et al., 2013).

(B) ChIP-qPCR results for H3K27ac and H3K4me1 at the promoter (P1 and P2), middle (M), and enhancer (E1 and E2) regions in BV2 cells treated with LPS (1 μg/mL).

(C) Profile of NF-κB p65 binding at the *Tet2* promoter and upstream regions after 1 h treatment of macrophages with KLA, generated from published ChIP-seq data (Kaikkonen et al., 2013).

(D) ChIP-qPCR results for NF-κB p65 in the same regions as in (B) in BV2 cells treated with LPS (1 μg/mL).

Tet2 middle region (M) represents a region between the promoter and the enhancer used as negative control for ChIP. Data represented as mean ± SD. The results in (B) are the average of three (for H3K4me1) and four (for H3K27ac) independent experiments. The results in (D) are the average of three independent experiments. Statistical analysis was performed using two-tailed Student's t test. *$p < 0.05$ and **$p < 0.01$.

See also Figure S2.

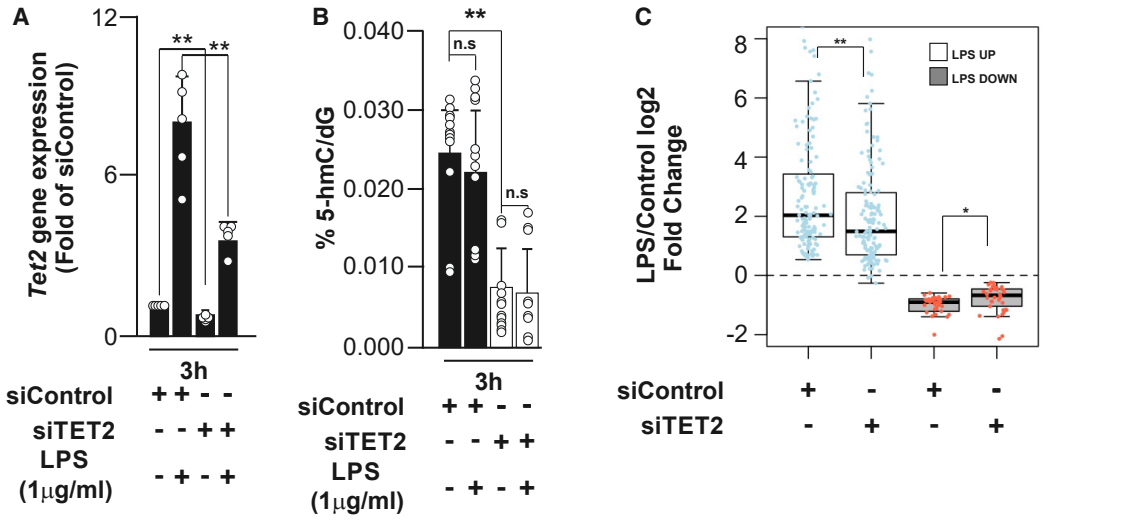

D

	GO Term (in LPS treated cells):	*p*-value	Enrichment
Downregulated	Innate Immune Response	6.90E-26	12.21
	Immune Response	1.10E-25	8.00
	Immune System Process	4.90E-24	5.12
	Defence Response	1.40E-22	6.89
	Response to Interferon Beta	5.30E-18	68.42
Upregulated	Cell Cycle	1.50E-12	9.75
	Cell Cycle Process	1.50E-12	12.24
	DNA replication	1.40E-08	25.64
	DNA metabolic process	1.90E-07	10.74
	Mitotic Cell Cycle	5.40E-07	11.32

E

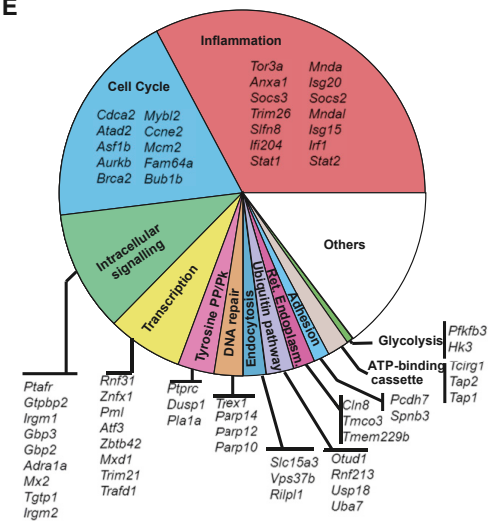

F

	GO Term (in Basal conditions):	*p*-value	Enrichment
Downregulated	Immune system process	1.10E-10	3.54
	Immune Response	1.30E-6	4.10
	Positive regulation of response to stimulus	1.30E-6	3.33
	Regulation of immune system process	2.20E-6	3.95
	Positive regulation of biological process	3.70E-6	2.04
Upregulated	Cell Cycle	<1.00E-30	8.59
	Cell Cycle Process	<1.00E-30	9.48
	Mitotic cell cycle process	<1.00E-30	12.26
	Mitotic cell cycle	<1.00E-30	11.33
	Nuclear division	<1.00E-30	13.68

(legend on next page)

performed TET2 ChIP-qPCR. Our data show that, indeed, TET2 binding increases substantially at target genes upon LPS treatment, whereas a control locus (*Oct4*) shows no alterations (Figure 4G). Importantly, LPS-driven TET2 recruitment can be reversed upon knockdown of *Tet2* (Figure 4H; Figure S4H). These results suggest that TET2 acts directly on these genes but that its effect upon LPS is not predominantly mediated through its catalytic activity.

TET2 Regulates the "Classical" Inflammatory Response and the Metabolic Reprogramming Induced by LPS

The RNA-seq data suggested that TET2 plays a role in the LPS-induced inflammatory response, in particular the response to IFN-β (or type I IFN response) (Figure 3E). It was previously shown that TET2 is required for the repression of IL-6 upon LPS treatment in peripheral macrophages to ensure termination of inflammation (Zhang et al., 2015). IL-6 expression was unchanged in our RNA-seq, which was performed 3 h after LPS treatment. Given that 3 h is too early for the inflammatory resolution process to start, we analyzed the expression levels of IL-6 and other players related to the "classical" proinflammatory response (IL-1β and NOS-2 expression) at later time points upon LPS treatment (Figures 5A–5E). We observed in BV2 cells that although there was no difference at 3 h after LPS treatment, the expression of *Il-1β*, *Il-6* and *Nos-2* was reduced at 6 and 24 h post-LPS treatment upon TET2 depletion (Figures 5A–5C). Knockdown of TET2 led to significantly less IL-6 release into the media upon LPS treatment at 6 and 24 h in BV2 cells (Figure 5D).

To validate our observations in primary microglia cell cultures, we crossed conditional *Tet2* floxed mice ($Tet2^{flox/flox}$) with *Cx3cr1 Cre* mice ($Cx3cr1^{CreERT2/WT}$) to enable the production of inducible microglia-specific deletion of *Tet2* (Figures S5A–S5C). We isolated primary microglia from both $Tet2^{flox/flox}Cx3cr1$ Cre-positive (henceforth referred to as $Tet2^{flox/flox}Cx3cr1^{Cre/WT}$) and negative mice (referred as $Tet2^{flox/flox}Cx3cr1^{WT/WT}$) and treated cells with 4-OH-tamoxifen for 48 h, producing a partial genomic deletion of *Tet2* (Figures S5A and S5B). Importantly, this led to decreased *Tet2* expression in $Tet2^{flox/flox}Cx3cr1^{Cre/WT}$ in basal conditions and complete abrogation of *Tet2* upregulation upon treatment with 100 ng/mL of LPS for 24 h (Figure S5C). To analyze the effects of *Tet2* deletion over the inflammatory response, we compared the expression levels of different proinflammatory markers between primary $Tet2^{flox/flox}Cx3cr1^{Cre/WT}$ and $Tet2^{flox/flox}Cx3cr1^{WT/WT}$ microglia in response to LPS. In accordance with our results from BV2 cells, *Nos-2* expression decreased by about 50% in $Tet2^{flox/flox}Cx3cr1^{Cre/WT}$ compared with $Tet2^{flox/flox}Cx3cr1^{WT/WT}$ primary microglia 24 h after LPS challenge (Figure 5E). We also analyzed the release of IL-6 and TNF-α into the media 24 h after LPS treatment and observed a statistically significant inhibition of IL-6 release and TNF-α in primary microglia cell cultures supernatants (Figures 5F and 5G).

Collectively, our data suggest that in microglial cells, TET2 is not involved in the resolution of the inflammatory response as reported in peripheral immune cells (Zhang et al., 2015). Instead, microglial TET2 modulates the classical inflammatory response upon direct stimulus by LPS treatment. However, this time-dependent effect of TET2 on the LPS-induced expression of "classical" proinflammatory markers suggests an indirect effect. Therefore, we aimed to dissect the mechanisms that could affect the delayed expression of different inflammatory cytokines in activated microglia. TLR-4 stimulation induces a rapid and robust transcriptional response that involves genes that regulate metabolic reprogramming (Medzhitov and Horng, 2009). Treatment with LPS in macrophages and dendritic and microglia cells provokes a metabolic shift from oxidative phosphorylation (OXPHOS) toward aerobic glycolysis, a process required to quickly supply high-energy demands of the inflammatory response (Ruiz-García et al., 2011; Galván-Peña and O'Neill, 2014; Ganeshan and Chawla, 2014; Orihuela et al., 2016).

In proinflammatory (M1) macrophages, aerobic glycolysis is a consequence of glucose uptake and the conversion of pyruvate into lactate (Galván-Peña and O'Neill, 2014). Interestingly, two of the targets that were deregulated by *Tet2* knockdown in our RNA-seq data were hexokinase 3 (*Hk3*) and 6-phosphofructo-2-kinase/fructose-2,6-biphosphatase 3 (*Pfkfb3*), both playing an important role during the aerobic glycolysis process (Ruiz-García et al., 2011; Galván-Peña and O'Neill, 2014). We therefore asked if TET2 was involved in the early stages of the metabolic reprogramming induced by LPS. In BV2 cells, we measured the extracellular acidification rate (ECAR) as an indicator of lactate production and the mitochondrial oxygen consumption rate (OCR) as an indicator of the mitochondrial energy production in siControl and siTET2 BV2 cells with and without LPS at different time points (Figures 5H and 5I). A functional bioenergetics profile of siControl, siTET2 cells with and without LPS treatment in response to sequential treatment with oligomycin, FCCP, and rotenone/antimycin A was carried out (Figures S5D and S5E). Our results show reduced lactate production after *Tet2* knockdown at 3 and 24 h of LPS treatment at basal conditions (Figure 5H) and after oligomycin treatment, indicating reduced glycolysis (Figure S5D). We then asked whether this decrease in lactate formation at 3 h was correlated with a decrease in the glucose consumption. We analyzed the extracellular glucose levels after 3 h LPS treatment and found that siControl LPS-treated cells consume glucose from the media but that LPS-treated siTET2 cells show a substantial reduction in the glucose uptake (Figure 5J). Because *Tet2* knockdown

Figure 3. TET2 Regulates Signaling Pathways Induced by LPS

(A and B) Effect of siRNA Tet2 knockdown on *Tet2* gene expression (A) and on the global levels of 5hmC (B) with or without 3 h treatment with LPS (1 μg/mL).
(C) Expression change of LPS-responsive TET2-regulated genes (see Venn diagrams in Figure S3B) upon LPS treatment in siRNA control and TET2-treated cells.
(D) Table representing Gene Ontology (GO) analysis of all genes affected by *Tet2* knockdown after LPS treatment.
(E) Manual annotation representing different functional groups (and some examples of the genes) affected by *Tet2* knockdown after LPS treatment.
(F) Manual annotation representing different functional groups (and some examples of the genes) affected by *Tet2* knockdown under basal conditions.
Data shown are represented as mean ± SD from five (A) and three (B and C) independent experiments. Two-tailed Student's t test. *$p < 0.05$ and **$p < 0.01$.
See also Figure S3.

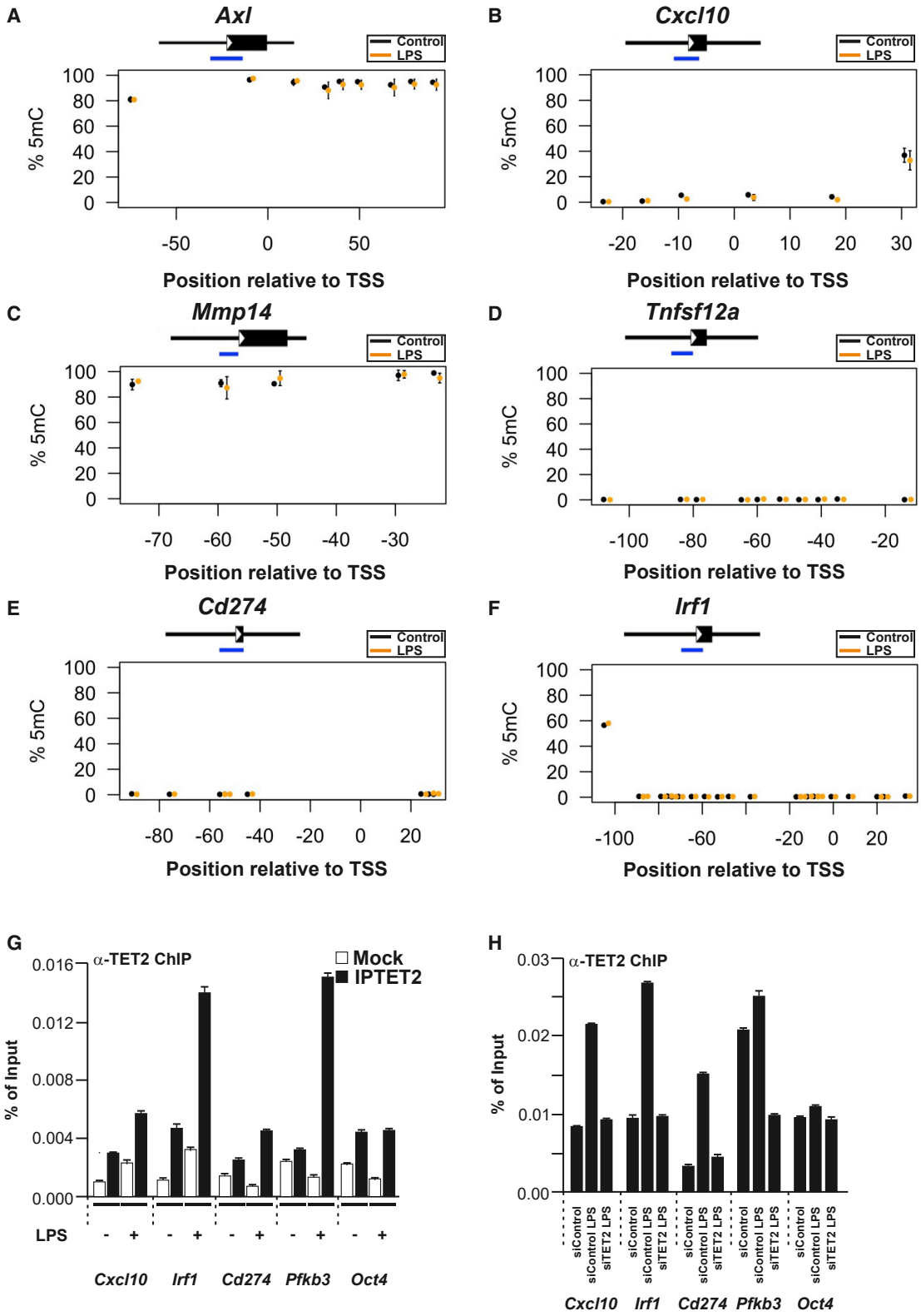

(legend on next page)

strongly reduced LPS-induced glycolysis, and because microglia have a metabolic dependence on glycolysis (Vilalta and Brown, 2014), we tested whether inhibition of glycolysis affected the inflammatory response. In agreement with our previous data, inhibition of hexokinase activity by using 2-deoxy-D-glucose (2-DG) inhibited the inflammatory response measured as NOS-2 expression in BV2 at 6 h without inducing cell death (Tannahill et al., 2013; Vilalta and Brown, 2014) (Figures S5F and S5G). These results suggest that TET2 regulation of the inflammatory response might be mediated by the early changes in glycolysis induced by TET2. Indeed, TET2 knockdown reduced the basal and maximal oxygen consumption of the cells after 3 h LPS treatment (Figure 5I; Figure S5E), but after 24 h LPS treatment, the cellular oxygen consumption levels increased (Figure 5I). This indicates that TET2 mediates the substantial LPS-induced metabolic reprogramming of the cells, including an early rise in glycolytic and mitochondrial energy production, followed by a fall in mitochondrial energy production potentially mediated by the well-known inhibition of mitochondria by NO from NOS-2 (Bal-Price et al., 2002; Doulias et al., 2013; Kelly and O'Neill, 2015).

Effect of TET2 Depletion in Microglia Cells *In Vivo*

Our *in vitro* results using primary microglia cells and BV2 cell line suggest that TET2 is necessary for a full proinflammatory response. These results contrast with findings in peripheral macrophages after intraperitoneal injection *in vivo* (Zhang et al., 2015). We therefore assessed the effect of microglial TET2 depletion *in vivo*, using an inflammatory model based on intraperitoneal injection of LPS, in our *Tet2*$^{flox/flox}$*Cx3cr1*$^{Cre/WT}$ and *Tet2*$^{flox/flox}$Cx3cr1$^{WT/WT}$ mice (Figure S6A). It has been demonstrated that this *in vivo* model induces a well-defined microglial proinflammatory phenotype different from the recently characterized molecular signature of disease-associated microglia (DAM) (Bodea et al., 2014; Krasemann et al., 2017).

In our conditional inducible knockout (KO) mouse model, we achieved about a 40% decrease in the expression of TET2 at the protein level within microglial cells (Figures S6B and S6C). We first assessed the effect of TET2 depletion in microglia cells after intraperitoneal injection of LPS in the substantia nigra (SN) in *Tet2*$^{flox/flox}$*Cx3cr1*$^{Cre/WT}$ and *Tet2*$^{flox/flox}$Cx3cr1$^{WT/WT}$ mice (Figures 6A–6G). We observed that depletion of microglial TET2 failed to affect microglia cell density at physiological conditions. However, upon treatment with LPS, we observed a decrease in the proliferation rate in microglia lacking TET2 (Figures 6A and 6B). This result is supported by our RNA-seq in BV2 cells, where we showed that several genes involved in cell cycle regulation were under control of TET2. Microglia activation is well known to be associated with prominent morphological alterations. Although homeostatic microglia are highly ramified cells, upon activation, microglia increase cell body and Iba1 expression, along with thickening of processes to end in complete retraction of cytoplasmic processes to acquire an amoeboid morphology. In response to repeated systemic LPS injections, a massive appearance of microglia exhibiting typical morphological features of activation was found 24 h after LPS challenge (Figure 6A). This observation prompted us to perform a detailed analysis of microglia on the basis of morphological features of homeostatic microglia and three well-defined states of microglia activation, as shown in Figure 6C. TET2 deletion did not alter the density of homeostatic microglia in healthy unlesioned brain (Figure 6C). In response to LPS, *Tet2*$^{flox/flox}$*Cx3cr1*$^{WT/WT}$ mice showed very low presence of homeostatic microglia, with very robust increases of activated microglial cells (Figure 6C). *Tet2*$^{flox/flox}$*Cx3cr1*$^{Cre/WT}$ mice showed significantly lower degree of microglia activation, affecting the number of reactive microglia cells (Figure 6C). A typical early feature of activated microglia is cell proliferation (Mathys et al., 2017), hence an effect of TET2 in cell cycle regulation cannot be discarded in response to proinflammatory challenge, in line with our RNA-seq data. We next dissected out the SN and extracted mRNA to measure the expression of different cytokines. TET2 knockdown in microglia cells failed to affect the expression of *Il-1β*, *Tnf-α*, and *Nos-2* in response to systemic LPS (Figure S6D). It is, however, important to note that in this *in vivo* model, microglia are not directly activated by LPS binding to TLR-4 but by different factors released by activated peripheral immune cells (Chen et al., 2012). We therefore also analyzed the effect of TET2 deletion on genes that become highly expressed after intraperitoneal injection with LPS. On the basis of publicly available data in this model (Krasemann et al., 2017), we focused on the expression of the two highest induced genes upon repeated systemic LPS injections, *Ptgs2* and *Cybb* (also known as *Cox-2* and *Nox-2*, respectively), both of which are considered proinflammatory mediators (Benusa et al., 2017; Alhadidi and Shah, 2018). Although no difference in expression was found with *Nox-2* expression in LPS-treated TET2-depleted mice (Figure 6D), there was a very strong inhibition of the LPS-induced COX2 expression in TET2-depleted microglia cells at both mRNA and protein levels (Figures 6E–6G).

Altogether these results suggest that TET2 plays a proinflammatory role in microglia (opposite to peripheral immune cells) and highlight potential differences in the role of TET2 in the inflammatory response between microglia and peripheral immune cells (London et al., 2013; Burm et al., 2015; Zarruk et al., 2018), suggesting that the action of TET2 is highly context specific.

Figure 4. TET2 Binds to the Promoter Regions of Several Target Genes

(A–F) Quantification of 5mC levels by oxBS-seq of the promoters of target genes after 3 h LPS (1 μg/mL) treatment. Blue bars indicate the position of the analyzed amplicons. Quantification of 5mC levels by oxBS-seq of the promoters of *Axl* (A), *Cxcl10* (B), *Mmp14* (C), *Tnfsf12a* (D), *Cd274* (E), and *Irf1* (F) after 3 h LPS (1 μg/mL) treatment. Blue bars indicate the position of the analyzed amplicons.

(G) TET2 ChIP for target genes after 3 h LPS treatment.

(H) TET2 ChIP of the genes after 3 h treatment with LPS (1 μg/mL) in control and TET2-depleted cells. *Oct4* was used as a negative control.

Data shown in (A)–(H) represent the mean ± SD of two technical replicates. Results from an independent biological replicate of data in (H) are shown in Figure S4H. Statistical analysis was performed using two-way ANOVA with a Tukey correction taking into account all CpGs for (A)–(F).

See also Figure S4.

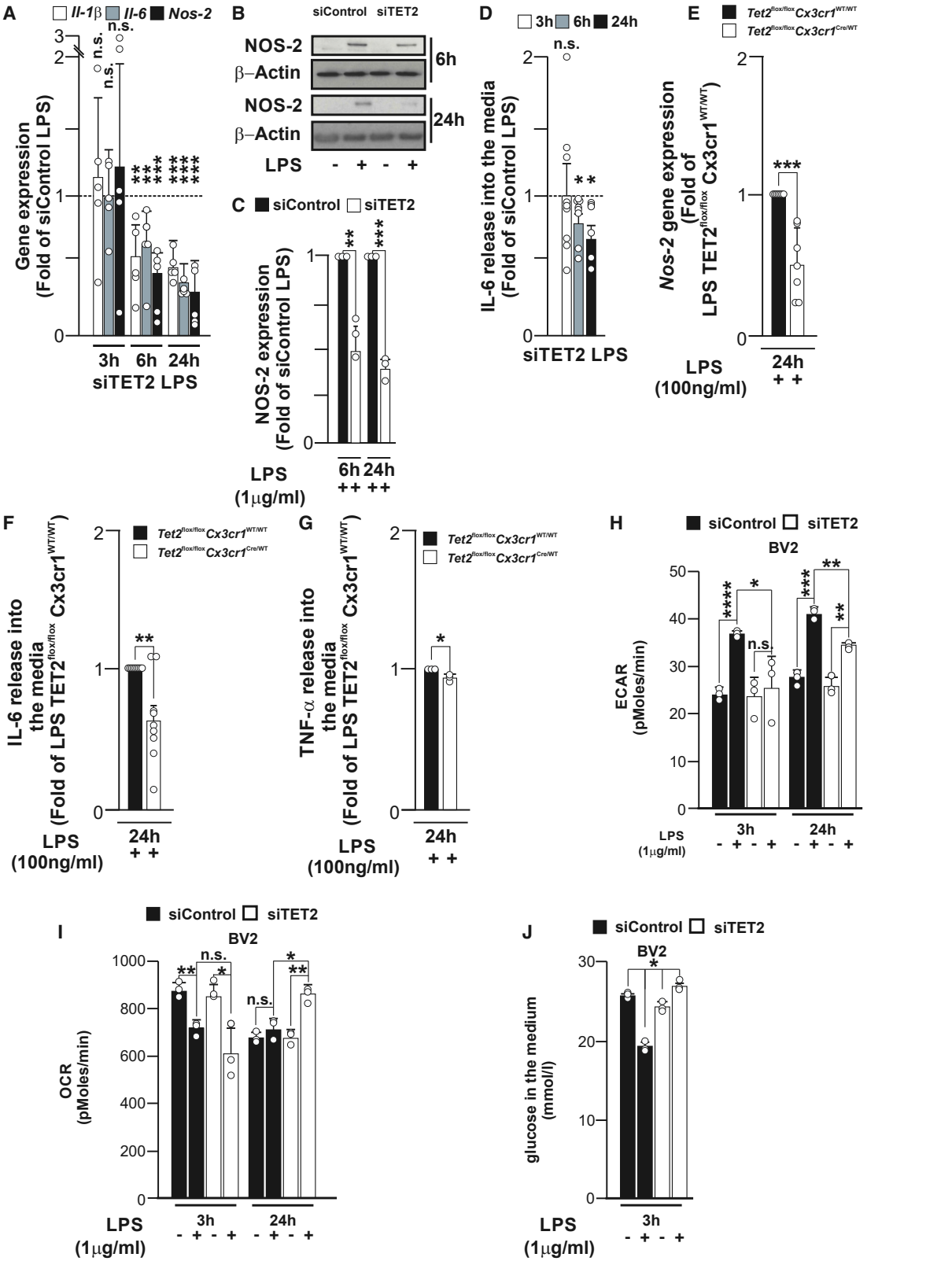

(legend on next page)

Microglial TET2 Expression during the Neurodegenerative Process

We and others (Janova et al., 2016), have observed that *Tet2* expression is induced under inflammatory conditions mediated by different TLR agonists and fibronectin (Figures S1A–S1C). Our next step was to test whether *Tet2* expression could also be affected by different pathological protein aggregates seen in a number of neurodegenerative diseases (Ugalde et al., 2016). For instance, α-synuclein aggregates induce microglial activation (Boza-Serrano et al., 2014) in a TLR-4-dependent manner (Fellner et al., 2013). Similarly, the fibrillar and oligomeric Aβ induce also a TLR-4-dependent immune response (Reed-Geaghan et al., 2009; Wang et al., 2018). BV2 cells were treated with α-synuclein aggregates and Aβ oligomers for 6 h, which produced an increase of *Tet2* expression similar to that observed with LPS (Figure S7A). To test whether microglial TET2 is upregulated *in vivo*, we analyzed TET2 expression in 18-month-old 5xFAD mice, which recapitulate many features of AD (Oakley et al., 2006). We observed that plaque-associated microglia in hippocampus displayed increased TET2 expression compared with homeostatic microglia located further from the plaques (Figures 7A and 7B; Figure S7B).

Finally, to test the clinical relevance of these results, we analyzed TET2 expression in post-mortem temporal cortex tissue from three AD subjects (Figures 7C–7E). We measured the fluorescent intensity of TET2 expression in Iba-1-positive microglial cells associated with Aβ plaques. These values were compared with TET2 expression in Iba-1-positive microglial cells located in the white matter and therefore not associated with plaques. Our analysis showed that in one subject (subject 1), there was significant upregulation of TET2 in plaque-associated microglia, while no statistical significance was observed in the other two subjects (Figure 7D). The discrepancy in the human samples cannot be directly linked to age, gender, or Braak stage (Figure 7E), and more thorough studies are needed to clarify these differences. Of note, plaques in AD subjects are very heterogeneous (unlike 5xFAD mice), which may explain the difference in microglial TET2 among the three subjects. Also, many TET2-positive cells did not colocalize with Iba-1-positive cells (Figure 7D). On the basis of their morphology, these TET2-positive/Iba-1-negative cells could be neurons, as previously reported (Dzitoyeva et al., 2008; Mi et al., 2015). We observed that the ratio of Iba-1+ to TET2+ cells varies within the three subjects. Although all the subjects present some Iba-1-positive cells expressing TET2, the numbers vary greatly within the three subjects. The Iba-1+/TET2+ ratio is relatively high in subject number 1, but on the other hand, subjects 2 and 3 present lower ratios (Figure 7D). Importantly, similar to the result obtained in the 5xFAD mouse model, in one of the subjects, microglial TET2 expression is highly expressed in the plaque-associated microglia (DAM), whereas microglia localized away from the plaques (homeostatic) showed little or no induction of TET2 expression (Figures 7A–7D). This differential response of TET2 expression in microglia cells depending on the distance to the plaque suggests that Aβ might also be a direct or indirect inducer of TET2 expression over time. However, more comprehensive studies are necessary to assess the impact of microglial TET2 in AD.

DISCUSSION

Epigenetic mechanisms mediated by TET2 have been proposed to regulate distinct aspects of the inflammatory response in different immune cell types. The potential involvement of TET2 in the recently characterized DAM (Keren Shaul et al., 2017; Krasemann et al., 2017) is deduced from our analysis of both AD transgenic mice and human AD tissues in which TET2 was highly upregulated specifically in plaque-associated microglia. We found that TET2 regulates primarily genes involved in the innate immune response and, more specifically, genes related to the TLR-induced type I IFN response (Noppert et al., 2007; Luu et al., 2014). Traditionally, the type I IFN response was considered solely a defense against viral and bacterial infections (Stifter and Feng, 2015; Kovarik et al., 2016). However, there is an increasing number of reports showing activation in the brain of the type I IFN response in ischemia (McDonough et al., 2017), spinal cord injury (Impellizzeri et al., 2015), and 5xFAD (Landel et al., 2014) and APP/PS1 (Taylor et al., 2014) AD mouse models, and in AD patients (Taylor et al., 2014). Using single-cell RNA-seq of microglia at different stages in a severe neurodegeneration model for AD (Mathys et al., 2017), the authors described that "late-stage" activated microglia highly express many type I and type II IFN response genes. Incidentally, and similar to our data, Gene Ontology analysis shows an enrichment in the expression of genes controlling cell cycle in "early-stage" activated microglia. These results highlight the similarity of the TET2-regulated inflammatory response in our experimental conditions with other neurodegenerative models.

Figure 5. TET2 Modulates LPS-Induced Changes in Cellular Metabolism and Inflammatory Response in Microglia Cells

(A) Graph showing the gene expression of *Il-1β*, *Nos-2*, and *Il-6* in LPS-treated BV2 cells with or without TET2 gene knockdown at different time points.

(B) and C) Representative immunoblot (B) and quantification (C) of NOS-2 protein at 6 and 24 h LPS treatment in BV2 cells transfected with siRNA control and siRNA *Tet2*.

(D) Quantification of IL-6 release into the media upon LPS treatment at different times (3, 6 and 24 h).

(E) Analysis of *Nos-2* gene expression in primary microglia cells after 24 h treatment with LPS.

(F and G) Histograms showing the effect of TET2 gene knockdown over IL-6 (F) and TNF-α (G) in LPS-treated primary microglia cells.

(H–J) Histograms showing the extracellular acidification rate (ECAR) (H), oxygen consumption rate (OCR) (I), and concentration of glucose (J) in the media in BV2 cells treated at different times with LPS.

Data shown are mean ± SD of five (A) and three (C) independent experiments. Data shown in (D) are mean ± SEM of nine (3 h), six (6 h), and eight (24 h) independent experiments. Data shown in (E) are mean ± SD of seven independent experiments. Data shown in (F) and (G) are mean ± SEM of nine (F) and three (G) independent experiments. Data shown in (H)–(J) are mean ± SD of three independent experiments. Statistical analysis was performed using two-tailed Student's t test. *$p < 0.05$, **$p < 0.01$, ***$p < 0.001$, and ****$p < 0.0001$.

See also Figure S5.

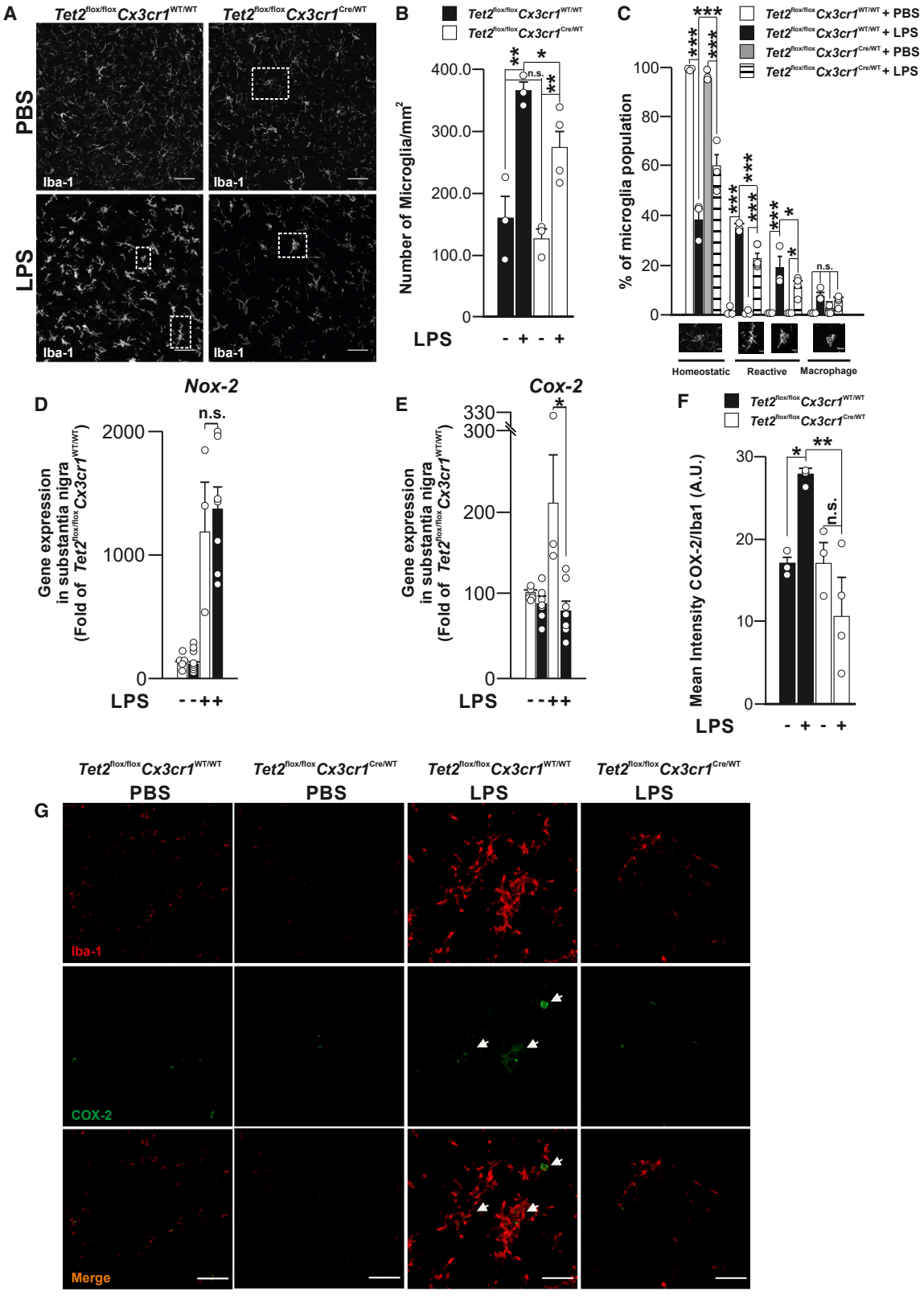

(legend on next page)

Notably, TET2 has been shown to terminate the inflammatory response in macrophages (Zhang et al., 2015). Using the same *in vivo* model used by the authors, we observe that upregulation of TET2 in microglia is necessary for a full proinflammatory response.

How does TET2 influence the late phase of the classical inflammatory response? The type I IFN response plays an important role in the TLR-induced classical inflammatory response (Luu et al., 2014; Taylor et al., 2014). One of the TET2-regulated genes that forms part of this response is the IFN-induced protein with tetratricopeptide repeats 2 (IFIT2), which amplifies the secretion of TNF-α and IL-6 *in vivo* in an endotoxin shock model (Siegfried et al., 2013). Additionally, TET2 regulates a number of small IFN-induced GTPases, in particular guanylate-binding proteins (GBPs), which are required for the full activation of the non-canonical caspase-11 inflammasome activation (Meunier et al., 2014). IFIT2, GBP2, and GBP3 appear in our RNA-seq analysis as genes under TET2 control upon LPS treatment, which could potentially affect the inflammatory response.

Our data also suggest that TET2 could regulate the classical inflammatory response through modulation of LPS-induced changes in metabolism. LPS causes a major shift in the metabolism of immune cells from OXPHOS toward aerobic glycolysis (a process known as the Warburg effect) (Rodríguez-Prados et al., 2010; Orihuela et al., 2016). We found that TET2 depletion leads to reduced glucose consumption and lactate production, an effect that precedes the reduction in classic inflammatory markers. Two genes known to regulate glycolysis (*Hk3* and *Pfkfb3*) are regulated by TET2 upon LPS treatment. HK3 catalyzes the first committed step of glycolysis (Nishizawa et al., 2014), while PFKFB3 catalyzes both the synthesis and degradation of fructose-2,6-bisphosphate (F2,6BP), a regulatory molecule that controls glycolysis in eukaryotes. Direct inhibition of glycolysis (using 2-D-deoxyglucose to inhibit hexokinase activity) prevented LPS induction of NOS-2, suggesting that the TET2 regulation of glycolysis may mediate the LPS-induced inflammatory response.

We also found that microglial TET2 is upregulated *in vivo* in two different models: in a neuroinflammatory mouse model induced by repeated intraperitoneal injections of LPS (Bodea et al., 2014; Krasemann et al., 2017) and in AD, including human subjects and transgenic mice (5xFAD). In AD, upregulated TET2 was restricted to plaque-associated microglia, which has been largely associated with AD pathogenesis. AD is characterized by the accumulation of aggregated proteins with immunogenic properties over DAM (Keren-Shaul et al., 2017; Krasemann et al., 2017; Mathys et al., 2017), which is strictly confined to Aβ plaques (Keren-Shaul et al., 2017). Interestingly, different single-cell RNA-seq of microglia in different AD models showed no upregulation of TET2 (Keren-Shaul et al., 2017; Krasemann et al., 2017; Mathys et al., 2017). However, our analysis using an antibody against TET2 (validated in KO mice) in human AD and 5xFAD mice demonstrated upregulation of TET2 in disease plaque-related microglia but not in homeostatic microglia. This suggests that increased levels of TET2 protein present in microglia cells might result from a post-translational mechanism (e.g., decrease in the rate of protein degradation).

Our results support the idea that TET2 could drive the proinflammatory activation of microglia and induction of metabolic reprogramming upon inflammatory stimulus. TET2 may become a potential drug target to control exacerbated neuroinflammatory response in different neurodegenerative diseases.

STAR★METHODS

Detailed methods are provided in the online version of this paper and include the following:

- KEY RESOURCES TABLE
- LEAD CONTACT AND MATERIALS AVAILABILITY
- EXPERIMENTAL MODEL AND SUBJECT DETAILS
  - Cell Lines and siRNA Transfection
  - Animals and Subject tissue
- METHOD DETAILS
  - Generation of microglia Tet2-deficient mice
  - Primary microglia cell culture preparations
  - RT-qPCR analysis
  - Immunofluorescence for mouse material
  - Immunofluorescence for the subject material
  - RNA-seq
  - OxBS-seq
  - Measurements of OCR and ECAR
  - Measurement of extra-cellular glucose
  - Preparation of α-synuclein and Aβ-oligomers
  - Immunoblotting
  - Microglia cell counting
  - Apoptosis determination
  - Cell viability
  - Chromatin Immunoprecipitation
  - Liquid chromatography-mass spectrometry
  - Microglia morphology
  - Images quantification
- QUANTIFICATION AND STATISTICAL ANALYSIS
- DATA AND SOFTWARE AVAILABILITY

Figure 6. Abrogation of *Tet2* in Microglia Cells Decreases the LPS-Induced Immune Response *In Vivo*

(A–C) Iba-1 immunostaining in substantia nigra of *Tet2*$^{flox/flox}$*Cx3cr1* $^{Cre/WT}$ and *Tet2*$^{flox/flox}$Cx3cr1$^{WT/WT}$ mice treated for 4 days either with LPS or vehicle (PBS) and sacrificed 24 h later (A) and analysis of microglia cell numbers (B) and activation status on the basis of morphology (C).

(D and E) qRT-PCR analysis of *Nox-2* (D) and *Cox-2* (E) in *Tet2*$^{flox/flox}$*Cx3cr1* $^{Cre/WT}$ and *Tet2*$^{flox/flox}$Cx3cr1$^{WT/WT}$ mice treated for 4 days either with LPS or vehicle (PBS) and sacrificed 24 h later.

(F and G) Quantification of Cox-2 staining (F) in Iba-1-positive cells (G) in the same type of mice.

Data represented as mean ± SEM. The results correspond to three independent experiments in (B) and (C). In (D) and (E), the number of independent experiments is equal to three for *Tet2*$^{flox/flox}$*Cx3cr1*$^{WT/WT}$ + LPS and seven for *Tet2*$^{flox/flox}$*Cx3cr1*$^{Cre/WT}$ + LPS. In (G), all treatments are three independent experiments except *Tet2*$^{flox/flox}$*Cx3cr1*$^{Cre/WT}$ + LPS, which is four independent experiments. Statistical analysis was performed using one-way ANOVA with a Student-Newman-Keuls post hoc test (C and G) or two-tailed Student's t test (D and E). *$p < 0.05$, **$p < 0.01$, ***$p < 0.01$. Scale bar in (A) is 10 μm and in (G) is 20 μm.

See also Figure S6.

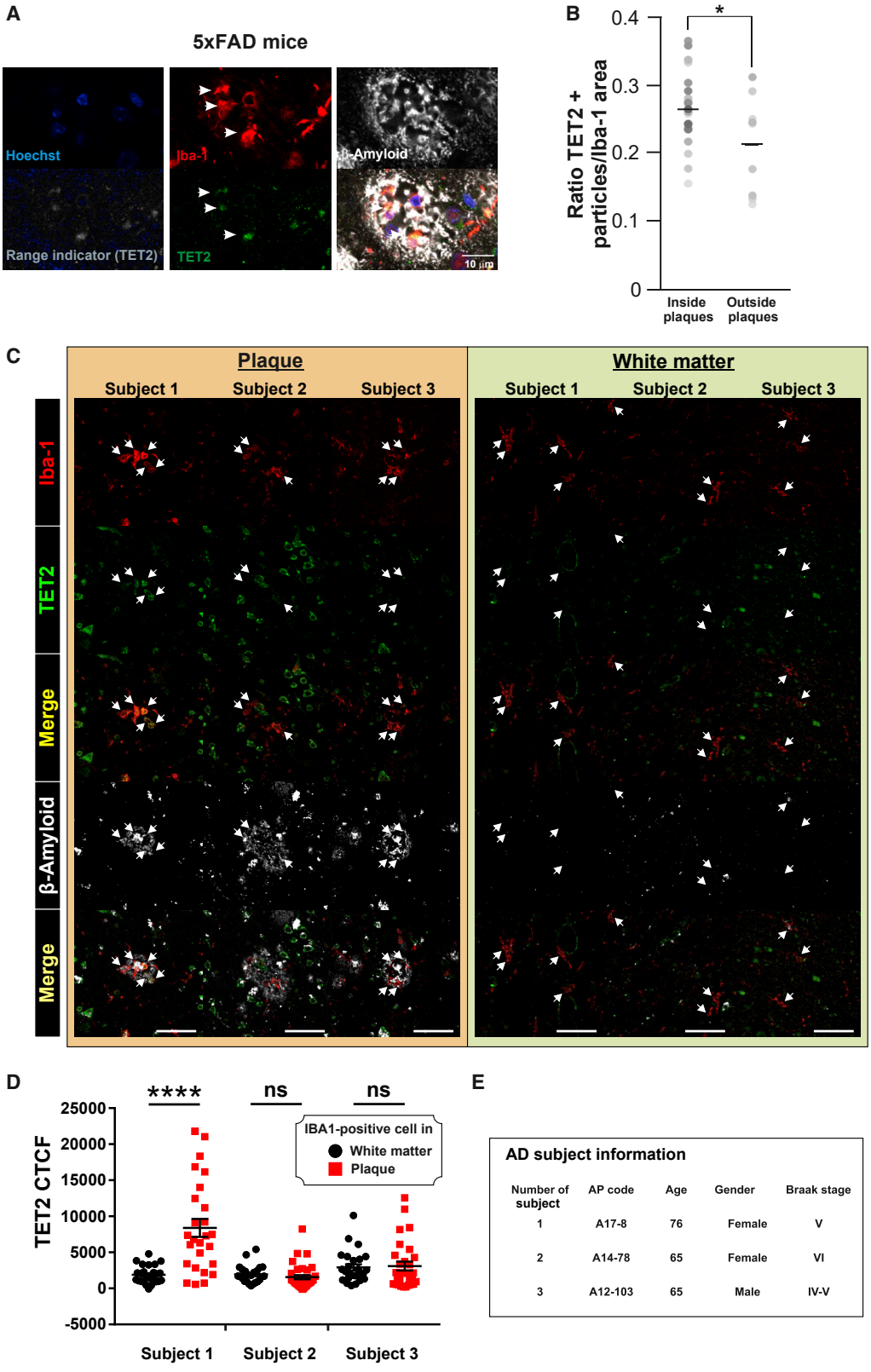

(legend on next page)

SUPPLEMENTAL INFORMATION

Supplemental Information can be found online at https://doi.org/10.1016/j.celrep.2019.09.013.

Received: October 24, 2017
Revised: April 18, 2019
Accepted: September 6, 2019
Published: October 15, 2019

ACKNOWLEDGMENTS

We would like to thank to Dr. de la Rica (Queen Mary University of London) for technical support and Dr. Hornedo-Ortega (University of Seville) for providing us with the α-synuclein. A.C.-J. is supported by a pre-doctoral fellowship from the Spanish Ministerio de Educación, Cultura y Deporte. Ö.D. has received funding from the People Programme (Marie Curie Actions) of the European Union's Seventh Framework Programme (FP7/2007-2013) under REA grant agreement 608765. M.V.N.-C. received a Children with Cancer UK fellowship (14-178). This work was supported by grants from Blizard Research Theme grants Queen Mary University of London; Blizard Institute; Spanish Ministerio de Ciencia, Innovación y Universidades/FEDER/UE RTI2018-098645-B-100; Swedish Research Council; ERA-NET TracInflam; Swedish Brain Foundation; and Karolinska Institutet Foundations. M.R.B. is a Sir Henry Dale Fellow (101225/Z/13/Z), jointly funded by the Wellcome Trust and the Royal Society. M.A.B. has been funded by the Barts Charity Centre for Trauma Sciences (C4TS), the Wellcome Trust Institutional Strategic Support Fund (ISSF), and the Spanish Ministry of Economy and Competitivity (Programa Ramón y Cajal: RYC-2017-21804).

AUTHOR CONTRIBUTIONS

M.A.B. and M.R.B. designed the study. A.C.-J., J.L.V., I.G.-D., J.G.-R., J.C.F.-M., and R.R. performed all the experiments with the *Tet2*$^{flox/flox}$; *Cx3Cr1*$^{Cre/wt}$ and *Tet2*$^{flox/flox}$; *Cx3Cr1*$^{wt/wt}$ mice. Ö.D. performed the ChIP analysis for NF-κB p65 and H3K27ac and H3K4me1 antibodies. Ö.D. and M.A.B. performed the ChIP analysis for TET2 antibody. M.V.N.-C. determined the ECAR and OCR index and glucose consumption in BV2 cells. K.B.-S. performed the oxBS sequencing experiments. V.S. and X.S. performed the staining and analysis of TET2 expression in AD subjects. R.A. and P.H. performed the mass spectrometry analysis for global levels of 5mC and 5hmC. A.V. and G.C.B. performed the analysis of TET2 in rat postnatal primary microglia. P.K.Y. performed the analysis of TET2 in mouse adult primary microglia. M.C. performed the analysis of TET2 in the human microglia cell line CHME3. R.R. performed the analysis of TET2 in the 5xFAD mice brain tissue and in *Tet2*$^{flox/flox}$; *Cx3Cr1*$^{WT/WT}$ and *Tet2*$^{flox/flox}$;*Cx3Cr1*$^{Cre/WT}$ injected with LPS. R.R. also performed the confocal analysis of microglia morphology and COX-2. A.M.S.-E. analyzed TET2/3 expression in BV2 cells after LTA treatment. K.T. and A.M.E.-O. and P.S.-H. analyzed the expression levels of TET2 in BV2 upon α-synuclein and β-oligomer treatments. E.R. provided the AD subject tissue. I.G.-D., J.G.-R., J.C.F.-M. performed the isolation of RNA from SN from mice injected with LPS and performed the qPCR analysis for the different cytokines and COX2 and NOX2. M.R.B. performed the RNA-seq experiments and analyzed the data. M.A.B. performed the qPCR analysis and immunoblots for the study of the inflammatory response in BV2 cells. J.L.V. and B.J. were involved in the study design. M.A.B. and M.R.B. wrote the manuscript with all the authors. All authors discussed the results and commented on or edited the manuscript.

DECLARATION OF INTERESTS

The authors declare no competing interests.

REFERENCES

Abeliovich, A., and Gitler, A.D. (2016). Defects in trafficking bridge Parkinson's disease pathology and genetics. Nature *539*, 207–216.

Alhadidi, Q., and Shah, Z.A. (2018). Cofilin mediates LPS-induced microglial cell activation and associated neurotoxicity through activation of NF-κB and JAK-STAT pathway. Mol. Neurobiol. *55*, 1676–1691.

Bal-Price, A., and Brown, G.C. (2001). Inflammatory neurodegeneration mediated by nitric oxide from activated glia-inhibiting neuronal respiration, causing glutamate release and excitotoxicity. J. Neurosci. *21*, 6480–6491.

Bal-Price, A., Matthias, A., and Brown, G.C. (2002). Stimulation of the NADPH oxidase in activated rat microglia removes nitric oxide but induces peroxynitrite production. J. Neurochem. *80*, 73–80.

Benusa, S.D., George, N.M., Sword, B.A., DeVries, G.H., and Dupree, J.L. (2017). Acute neuroinflammation induces AIS structural plasticity in a NOX2-dependent manner. J. Neuroinflammation *14*, 116.

Bodea, L.G., Wang, Y., Linnartz-Gerlach, B., Kopatz, J., Sinkkonen, L., Musgrove, R., Kaoma, T., Muller, A., Vallar, L., Di Monte, D.A., et al. (2014). Neurodegeneration by activation of the microglial complement-phagosome pathway. J. Neurosci. *34*, 8546–8556.

Bonasio, R., Tu, S., and Reinberg, D. (2010). Molecular signals of epigenetic states. Science *330*, 612–616.

Booth, M.J., Branco, M.R., Ficz, G., Oxley, D., Krueger, F., Reik, W., and Balasubramanian, S. (2012). Quantitative sequencing of 5-methylcytosine and 5-hydroxymethylcytosine at single-base resolution. Science *336*, 934–937.

Boza-Serrano, A., Reyes, J.F., Rey, N.L., Leffler, H., Bousset, L., Nilsson, U., Brundin, P., Venero, J.L., Burguillos, M.A., and Deierborg, T. (2014). The role of galectin-3 in α-synuclein-induced microglial activation. Acta Neuropathol. Commun. *2*, 156.

Branco, M.R., Ficz, G., and Reik, W. (2011). Uncovering the role of 5-hydroxymethylcytosine in the epigenome. Nat. Rev. Genet. *13*, 7–13.

Burguillos, M.A., Deierborg, T., Kavanagh, E., Persson, A., Hajji, N., Garcia-Quintanilla, A., Cano, J., Brundin, P., Englund, E., Venero, J.L., and Joseph, B. (2011). Caspase signalling controls microglia activation and neurotoxicity. Nature *472*, 319–324.

Burguillos, M.A., Svensson, M., Schulte, T., Boza-Serrano, A., Garcia-Quintanilla, A., Kavanagh, E., Santiago, M., Viceconte, N., Oliva-Martin, M.J., Osman, A.M., et al. (2015). Microglia-secreted galectin-3 acts as a toll-like receptor 4 ligand and contributes to microglial activation. Cell Rep. *10*, 1626–1638.

Burm, S.M., Zuiderwijk-Sick, E.A., 't Jong, A.E., van der Putten, C., Veth, J., Kondova, I., and Bajramovic, J.J. (2015). Inflammasome-induced IL-1β secretion in microglia is characterized by delayed kinetics and is only partially dependent on inflammatory caspases. J. Neurosci. *35*, 678–687.

Butovsky, O., Jedrychowski, M.P., Moore, C.S., Cialic, R., Lanser, A.J., Gabriely, G., Koeglsperger, T., Dake, B., Wu, P.M., Doykan, C.E., et al. (2014). Identification of a unique TGF-β-dependent molecular and functional signature in microglia. Nat. Neurosci. *17*, 131–143.

Chen, Z., Jalabi, W., Shpargel, K.B., Farabaugh, K.T., Dutta, R., Yin, X., Kidd, G.J., Bergmann, C.C., Stohlman, S.A., and Trapp, B.D. (2012).

Figure 7. Microglial TET2 Expression in 5xFAD Mice and Alzheimer's Disease Brain Tissue

(A–D) Colocalization analysis of TET2, Iba-1, and Aβ plaques in the hippocampus of 18-month-old 5xFAD mice (A and B) and three AD subjects (C and D).
(E) Details of age, gender, and Braak stage for each AD subject.
Data shown in (B) are mean ± SEM of three independent experiments. Arrowheads indicate microglial cells. In (D), each shape represents intensity from some single microglia found either in the white matter (black circles) or inside a plaque (red squares). Statistical analysis used for (B) was two-tailed Student's t test and for (D) was one-way ANOVA with Sidak's multiple-comparison test. CTCF, corrected total cell fluorescence. *$p < 0.05$ and ****$p < 0.0001$. Scale bar for (A) is 10 μm and for (C) is 50 μm.
See also Figure S7.

Lipopolysaccharide-induced microglial activation and neuroprotection against experimental brain injury is independent of hematogenous TLR4. J. Neurosci. *32*, 11706–11715.

Cho, S.-H., Chen, J.A., Sayed, F., Ward, M.E., Gao, F., Nguyen, T.A., Krabbe, G., Sohn, P.D., Lo, I., Minami, S., et al. (2015). SIRT1 deficiency in microglia contributes to cognitive decline in aging and neurodegeneration via epigenetic regulation of IL-1b. J. Neurosci. *35*, 807–818.

Cogswell, J.P., Godlevski, M.M., Wisely, G.B., Clay, W.C., Leesnitzer, L.M., Ways, J.P., and Gray, J.G. (1994). NF-kappa B regulates IL-1 beta transcription through a consensus NF-kappa B binding site and a nonconsensus CRE-like site. J. Immunol. *153*, 712–723.

Creyghton, M.P., Cheng, A.W., Welstead, G.G., Kooistra, T., Carey, B.W., Steine, E.J., Hanna, J., Lodato, M.A., Frampton, G.M., Sharp, P.A., et al. (2010). Histone H3K27ac separates active from poised enhancers and predicts developmental state. Proc. Natl. Acad. Sci. U S A *107*, 21931–21936.

Cull, A.H., Snetsinger, B., Buckstein, R., Wells, R.A., and Rauh, M.J. (2017). Tet2 restrains inflammatory gene expression in macrophages. Exp. Hematol. *55*, 56–70.e13.

de la Rica, L., Deniz, Ö., Cheng, K.C.L., Todd, C.D., Cruz, C., Houseley, J., and Branco, M.R. (2016). TET-dependent regulation of retrotransposable elements in mouse embryonic stem cells. Genome Biol. *17*, 234.

Deierborg, T. (2013). Preparation of primary microglia cultures from postnatal mouse and rat brains. In Microglia. Methods in Molecular Biology (Methods and Protocols), *Volume 1041*, B. Joseph and J. Venero, eds. (Humana Press).

Doulias, P.-T., Tenopoulou, M., Greene, J.L., Raju, K., and Ischiropoulos, H. (2013). Nitric oxide regulates mitochondrial fatty acid metabolism through reversible protein S-nitrosylation. Sci. Signal. *6*, rs1.

Dzitoyeva, S., Chen, H., and Manev, H. (2008). Effect of aging on 5-hydroxymethylcytosine in brain mitochondria. Neurobiol. Aging *86*, 3279–3288.

Fellner, L., Irschick, R., Schanda, K., Reindl, M., Klimaschewski, L., Poewe, W., Wenning, G.K., and Stefanova, N. (2013). Toll-like receptor 4 is required for α-synuclein dependent activation of microglia and astroglia. Glia *61*, 349–360.

Galván-Peña, S., and O'Neill, L.A.J. (2014). Metabolic reprograming in macrophage polarization. Front. Immunol. *5*, 420.

Ganeshan, K., and Chawla, A. (2014). Metabolic regulation of immune responses. Annu. Rev. Immunol. *32*, 609–634.

Hanisch, U.-K.K., and Kettenmann, H. (2007). Microglia: active sensor and versatile effector cells in the normal and pathologic brain. Nat. Neurosci. *10*, 1387–1394.

Hornedo-Ortega, R., Álvarez-Fernández, M.A., Cerezo, A.B., Richard, T., Troncoso, A.M.A., and Garcia-Parrilla, M.A.C. (2016). Protocatechuic acid: inhibition of fibril formation, destabilization of preformed fibrils of amyloid-β and α-synuclein, and neuroprotection. J. Agric. Food Chem. *64*, 7722–7732.

Ichiyama, K., Chen, T., Wang, X., Yan, X., Kim, B.S., Tanaka, S., Ndiaye-Lobry, D., Deng, Y., Zou, Y., Zheng, P., et al. (2015). The methylcytosine dioxygenase Tet2 promotes DNA demethylation and activation of cytokine gene expression in T cells. Immunity *42*, 613–626.

Impellizzeri, D., Ahmad, A., Di Paola, R., Campolo, M., Navarra, M., Esposito, E., and Cuzzocrea, S. (2015). Role of Toll like receptor 4 signaling pathway in the secondary damage induced by experimental spinal cord injury. Immunobiology *220*, 1039–1049.

Janova, H., Böttcher, C., Holtman, I.R., Regen, T., van Rossum, D., Götz, A., Ernst, A.S., Fritsche, C., Gertig, U., Saiepour, N., et al. (2016). CD14 is a key organizer of microglial responses to CNS infection and injury. Glia *64*, 635–649.

Kaikkonen, M.U., Spann, N.J., Heinz, S., Romanoski, C.E., Allison, K.A., Stender, J.D., Chun, H.B., Tough, D.F., Prinjha, R.K., Benner, C., and Glass, C.K. (2013). Remodeling of the enhancer landscape during macrophage activation is coupled to enhancer transcription. Mol. Cell *51*, 310–325.

Kelly, B., and O'Neill, L.A. (2015). Metabolic reprogramming in macrophages and dendritic cells in innate immunity. Cell Res. *25*, 771–784.

Keren-Shaul, H., Spinrad, A., Weiner, A., Matcovitch-Natan, O., Dvir-Szternfeld, R., Ulland, T.K., David, E., Baruch, K., Lara-Astaiso, D., Toth, B., et al. (2017). A unique microglia type associated with restricting development of Alzheimer's disease. Cell *169*, 1276–1290.e17.

Kovarik, P., Castiglia, V., Ivin, M., and Ebner, F. (2016). Type I interferons in bacterial infections: A balancing act. Front. Immunol. *7*, 652.

Krasemann, S., Madore, C., Cialic, R., Baufeld, C., Calcagno, N., El Fatimy, R., Beckers, L., O'Loughlin, E., Xu, Y., Fanek, Z., et al. (2017). The TREM2-APOE pathway drives the transcriptional phenotype of dysfunctional microglia in neurodegenerative diseases. Immunity *47*, 566–581.e9.

Krueger, F., and Andrews, S.R. (2011). Bismark: a flexible aligner and methylation caller for Bisulfite-Seq applications. Bioinformatics *27*, 1571–1572.

Lambertsen, K.L., Biber, K., and Finsen, B. (2012). Inflammatory cytokines in experimental and human stroke. J. Cereb. Blood Flow Metab. *32*, 1677–1698.

Landel, V., Baranger, K., Virard, I., Loriod, B., Khrestchatisky, M., Rivera, S., Benech, P., and Féron, F. (2014). Temporal gene profiling of the 5XFAD transgenic mouse model highlights the importance of microglial activation in Alzheimer's disease. Mol. Neurodegener. *9*, 33.

London, A., Cohen, M., and Schwartz, M. (2013). Microglia and monocyte-derived macrophages: functionally distinct populations that act in concert in CNS plasticity and repair. Front. Cell. Neurosci. *7*, 34.

Luu, K., Greenhill, C.J., Majoros, A., Decker, T., Jenkins, B.J., and Mansell, A. (2014). STAT1 plays a role in TLR signal transduction and inflammatory responses. Immunol. Cell Biol. *92*, 761–769.

Malik, M., Parikh, I., Vasquez, J.B., Smith, C., Tai, L., Bu, G., LaDu, M.J., Fardo, D.W., Rebeck, G.W., and Estus, S. (2015). Genetics ignite focus on microglial inflammation in Alzheimer's disease. Mol. Neurodegener. *10*, 52.

Mathys, H., Adaikkan, C., Gao, F., Young, J.Z., Manet, E., Hemberg, M., De Jager, P.L., Ransohoff, R.M., Regev, A., and Tsai, L.H. (2017). Temporal tracking of microglia activation in neurodegeneration at single-cell resolution. Cell Rep. *21*, 366–380.

Matt, S.M., Lawson, M.A., and Johnson, R.W. (2016). Aging and peripheral lipopolysaccharide can modulate epigenetic regulators and decrease IL-1β promoter DNA methylation in microglia. Neurobiol. Aging *47*, 1–9.

McCloy, R.A., Rogers, S., Caldon, C.E., Lorca, T., Castro, A., and Burgess, A. (2014). Partial inhibition of Cdk1 in G 2 phase overrides the SAC and decouples mitotic events. Cell Cycle *13*, 1400–1412.

McDonough, A., Lee, R.V., Noor, S., Lee, C., Le, T., Iorga, M., Phillips, J.L.H., Murphy, S., Möller, T., and Weinstein, J.R. (2017). Ischemia/reperfusion induces interferon stimulated gene expression in microglia. J. Neurosci. *37*, 8292–8308.

Medzhitov, R., and Horng, T. (2009). Transcriptional control of the inflammatory response. Nat. Rev. Immunol. *9*, 692–703.

Meunier, E., Dick, M.S., Dreier, R.F., Schürmann, N., Kenzelmann Broz, D., Warming, S., Roose-Girma, M., Bumann, D., Kayagaki, N., Takeda, K., et al. (2014). Caspase-11 activation requires lysis of pathogen-containing vacuoles by IFN-induced GTPases. Nature *509*, 366–370.

Mi, Y., Gao, X., Dai, J., Ma, Y., Xu, L., and Jin, W. (2015). A novel function of TET2 in CNS: Sustaining neuronal survival. Int. J. Mol. Sci. *16*, 21846–21857.

Moran-Crusio, K., Reavie, L., Shih, A., Abdel-Wahab, O., Ndiaye-Lobry, D., Lobry, C., Figueroa, M.E., Vasanthakumar, A., Patel, J., Zhao, X., et al. (2011). Tet2 loss leads to increased hematopoietic stem cell self-renewal and myeloid transformation. Cancer Cell *20*, 11–24.

Nishizawa, T., Kanter, J.E., Kramer, F., Barnhart, S., Shen, X., Vivekanandan-Giri, A., Wall, V.Z., Kowitz, J., Devaraj, S., O'Brien, K.D., et al. (2014). Testing the role of myeloid cell glucose flux in inflammation and atherosclerosis. Cell Rep. *7*, 356–365.

Noppert, S.J., Fitzgerald, K.A., and Hertzog, P.J. (2007). The role of type I interferons in TLR responses. Immunol. Cell Biol. *85*, 446–457.

Oakley, H., Cole, S.L., Logan, S., Maus, E., Shao, P., Craft, J., Guillozet-Bongaarts, A., Ohno, M., Disterhoft, J., Van Eldik, L., et al. (2006). Intraneuronal β-amyloid aggregates, neurodegeneration, and neuron loss in transgenic mice with five familial Alzheimer's disease mutations: potential factors in amyloid plaque formation. J. Neurosci. *26*, 10129–10140.

Orihuela, R., McPherson, C.A., and Harry, G.J. (2016). Microglial M1/M2 polarization and metabolic states. Br. J. Pharmacol. *173*, 649–665.

Park, G., Tan, J., Garcia, G., Kang, Y., Salvesen, G., and Zhang, Z. (2016). Regulation of Histone Acetylation by Autophagy in Parkinson Disease. J. Biol. Chem. *291*, 3531–3540.

Perry, V.H., and Holmes, C. (2014). Microglial priming in neurodegenerative disease. Nat. Rev. Neurol. *10*, 217–224.

Phipps, A.J., Vickers, J.C., Taberlay, P.C., and Woodhouse, A. (2016). Neurofilament-labeled pyramidal neurons and astrocytes are deficient in DNA methylation marks in Alzheimer's disease. Neurobiol. Aging *45*, 30–42.

Pickrell, A.M., and Youle, R.J. (2015). The roles of PINK1, parkin, and mitochondrial fidelity in Parkinson's disease. Neuron *85*, 257–273.

Ransohoff, R.M. (2016). How neuroinflammation contributes to neurodegeneration. Science *353*, 777–783.

Reed-Geaghan, E.G., Savage, J.C., Hise, A.G., and Landreth, G.E. (2009). CD14 and toll-like receptors 2 and 4 are required for fibrillar Abeta-stimulated microglial activation. J. Neurosci. *29*, 11982–11992.

Rodríguez-Prados, J.-C., Través, P.G., Cuenca, J., Rico, D., Aragonés, J., Martín-Sanz, P., Cascante, M., and Boscá, L. (2010). Substrate fate in activated macrophages: a comparison between innate, classic, and alternative activation. J. Immunol. *185*, 605–614.

Ruiz-García, A., Monsalve, E., Novellasdemunt, L., Navarro-Sabaté, A., Manzano, A., Rivero, S., Castrillo, A., Casado, M., Laborda, J., Bartrons, R., and Díaz-Guerra, M.J. (2011). Cooperation of adenosine with macrophage Toll-4 receptor agonists leads to increased glycolytic flux through the enhanced expression of PFKFB3 gene. J. Biol. Chem. *286*, 19247–19258.

Schafer, D.P., Lehrman, E.K., Kautzman, A.G., Koyama, R., Mardinly, A.R., Yamasaki, R., Ransohoff, R.M., Greenberg, M.E., Barres, B.A., and Stevens, B. (2012). Microglia sculpt postnatal neural circuits in an activity and complement-dependent manner. Neuron *74*, 691–705.

Shen, X., Burguillos, M.A., Osman, A.M., Frijhoff, J., Carrillo-Jiménez, A., Kanatani, S., Augsten, M., Saidi, D., Rodhe, J., Kavanagh, E., et al. (2016). Glioma-induced inhibition of caspase-3 in microglia promotes a tumor-supportive phenotype. Nat. Immunol. *17*, 1282–1290.

Siegfried, A., Berchtold, S., Manncke, B., Deuschle, E., Reber, J., Ott, T., Weber, M., Kalinke, U., Hofer, M.J., Hatesuer, B., et al. (2013). IFIT2 is an effector protein of type I IFN-mediated amplification of lipopolysaccharide (LPS)-induced TNF-α secretion and LPS-induced endotoxin shock. J. Immunol. *191*, 3913–3921.

Stifter, S.A., and Feng, C.G. (2015). Interfering with immunity: detrimental role of type I IFNs during infection. J. Immunol. *194*, 2455–2465.

Tannahill, G.M., Curtis, A.M., Adamik, J., Palsson-McDermott, E.M., McGettrick, A.F., Goel, G., Frezza, C., Bernard, N.J., Kelly, B., Foley, N.H., et al. (2013). Succinate is an inflammatory signal that induces IL-1β through HIF-1α. Nature *496*, 238–242.

Taylor, J.M., Minter, M.R., Newman, A.G., Zhang, M., Adlard, P.A., and Crack, P.J. (2014). Type-1 interferon signaling mediates neuro-inflammatory events in models of Alzheimer's disease. Neurobiol. Aging *35*, 1012–1023.

Trapnell, C., Pachter, L., and Salzberg, S.L. (2009). TopHat: discovering splice junctions with RNA-Seq. Bioinformatics *25*, 1105–1111.

Tsagaratou, A., González-Avalos, E., Rautio, S., Scott-Browne, J.P., Togher, S., Pastor, W.A., Rothenberg, E.V., Chavez, L., Lähdesmäki, H., and Rao, A. (2017). TET proteins regulate the lineage specification and TCR-mediated expansion of iNKT cells. Nat. Immunol. *18*, 45–53.

Ugalde, C.L., Finkelstein, D.I., Lawson, V.A., and Hill, A.F. (2016). Pathogenic mechanisms of prion protein, amyloid-β and α-synuclein misfolding: the prion concept and neurotoxicity of protein oligomers. J. Neurochem. *139*, 162–180.

Van Cauwenberghe, C., Van Broeckhoven, C., and Sleegers, K. (2016). The genetic landscape of Alzheimer disease: clinical implications and perspectives. Genet. Med. *18*, 421–430.

Vilalta, A., and Brown, G.C. (2014). Deoxyglucose prevents neurodegeneration in culture by eliminating microglia. J. Neuroinflammation *11*, 58.

Voloboueva, L.A., Emery, J.F., Sun, X., and Giffard, R.G. (2013). Inflammatory response of microglial BV-2 cells includes a glycolytic shift and is modulated by mitochondrial glucose-regulated protein 75/mortalin. FEBS Lett. *587*, 756–762.

Wang, S., Zhang, X., Zhai, L., Sheng, X., Zheng, W., Chu, H., and Zhang, G. (2018). Atorvastatin attenuates cognitive deficits and neuroinflammation induced by $A\beta_{1-42}$ involving modulation of TLR4/TRAF6/NF-κB Pathway. J. Mol. Neurosci. *64*, 363–373.

Watson, C.T., Roussos, P., Garg, P., Ho, D.J., Azam, N., Katsel, P.L., Haroutunian, V., and Sharp, A.J. (2016). Genome-wide DNA methylation profiling in the superior temporal gyrus reveals epigenetic signatures associated with Alzheimer's disease. Genome Med. *8*, 5.

Wu, Y., Dissing-Olesen, L., MacVicar, B.A., and Stevens, B. (2015). Microglia: dynamic mediators of synapse development and plasticity. Trends Immunol. *36*, 605–613.

Wüllner, U., Kaut, O., deBoni, L., Piston, D., and Schmitt, I. (2016). DNA methylation in Parkinson's disease. J. Neurochem. *139* (*Suppl 1*), 108–120.

Yip, P.K., Kaan, T.K., Fenesan, D., and Malcangio, M. (2009). Rapid isolation and culture of primary microglia from adult mouse spinal cord. J. Neurosci. Methods *183*, 223–237.

Zarruk, J.G., Greenhalgh, A.D., and David, S. (2018). Microglia and macrophages differ in their inflammatory profile after permanent brain ischemia. Exp. Neurol. *301* (*Pt B*), 120–132.

Zhang, Q., Zhao, K., Shen, Q., Han, Y., Gu, Y., Li, X., Zhao, D., Liu, Y., Wang, C., Zhang, X., et al. (2015). Tet2 is required to resolve inflammation by recruiting Hdac2 to specifically repress IL-6. Nature *525*, 389–393.

STAR★METHODS

KEY RESOURCES TABLE

REAGENT or RESOURCE	SOURCE	IDENTIFIER
Antibodies		
β-Actin (clone AC-74)	Sigma Aldrich	Cat.# A5316; RRID:AB_476743
β-Amyloid (clone 4G8)	Biolegend	Cat.# 800701; RRID:AB_2564633
β-Amyloid (clone BAM-10)	Sigma Aldrich	Cat.# A3981; RRID:AB_1078153
COX-2	R & D systems	Cat.# AF4198; RRID:AB_2229909
Donkey anti-Goat IgG, Alexa Fluor 568	Invitrogen	Cat# A-11057; RRID: AB_142581
Donkey anti-Rabbit IgG, Alexa Fluor 488	Invitrogen	Cat# A-21206; RRID: AB_141708
Donkey anti-Mouse IgG, CF633	Biotium	Cat# 20124; RRID: AB_10853607
Goat Anti-Mouse Immunoglobulins/HRP (affinity isolated)	Dako (Agilent)	Cat# P044701-2; RRID: AB_2617137
Goat Anti-Rabbit Immunoglobulins/HRP (affinity isolated)	Dako (Agilent)	Cat.# P044801-2; RRID: AB_2617138
Histone-3 (H3)	Abcam	Cat.# ab1791; RRID:AB_302613
H3K4me1	Diagenode	Cat.# C15410194; RRID:AB_2637078
H3K27ac	Diagenode	Cat.# C15410196; RRID:AB_2637079
Iba-1	Abcam	Cat.# ab5076; RRID:AB_2224402
Iba-1	Wako	Cat.# 019-19741; RRID:AB_839504
NF-κB p65 (C-20)	Santa Cruz Biotech.	Cat.# sc-372; RRID:AB_632037
NOS2 (M-19)	Santa Cruz Biotech.	Cat.# sc-650; RRID:AB_631831
TET2	Abcam	Cat.# ab94580; RRID:AB_10887588
TET2	Abcam	Cat.# ab124297; RRID:AB_2722695
Biological Samples		
Human Temporal lobes belonging to AD patients	University Hospital Virgen del Rocio, Seville (Spain)	A17-8, A14-78, A12-103
Chemicals, Peptides, and Recombinant Proteins		
LPS (from *Escherichia coli*, serotype 026:B6), *-in vitro* studies-.	Sigma Aldrich	Cat.# L8274
LPS (from Salmonella abortus equi S-form), *-in vivo* studies-.	Enzo LifeSciences	Cat.# ALX-581-009-L001
Lipofectamine 3000 Reagent	ThermoFisher Scientific	Cat.# L3000015
TRI Reagent®	Sigma Aldrich	Cat.# T9424
Autofluorescence Eliminator Reagent	Millipore	Cat.# 2160
RevertAid First Strand cDNA Synthesis Kit	ThermoFisher Scientific	Cat.# K1622
MESA BLUE qPCR 2X MasterMix Plus for SYBR®	Eurogentec	Cat.# 05-SY2X-03+WOUB
Potassium perruthenate(VII), 97% ($KRuO_4$)	Alfa Aesar	Cat. # 11877.03
Micro Bio-Spin Size Exclusion Spin Columns	Bio-Rad	Cat.# Micro Bio-Spin® Columns with Bio-Gel® P-XX
Target Retrieval Solution, Citrate pH 6.1 (10x)	Agilent	Cat.# S1699
Fluoromount-G	SouthernBiotech	Cat.# 0100-01
Seahorse XF24 Cell Culture Microplates	Agilent	Cat.# 0100-01100882-004
BD Cell-Tak	BD Biosciences	Cat.# 354240
Seahorse Bioscience XF Calibrant	Agilent	Cat.# 100840-000
Seahorse XF assay media	Agilent	Cat.# 102365-100
Oligomycin	Sigma-Aldrich	Cat.# 75351
FCCP	Sigma-Aldrich	Cat.# C2920

(*Continued on next page*)

Continued

REAGENT or RESOURCE	SOURCE	IDENTIFIER
Rotenone	Sigma-Aldrich	Cat.# R8875
Antimycin A	Sigma-Aldrich	Cat.# A8674
Human recombinant α-synuclein monomers	Alexo Tech AB	Cat.# AS-600-XX
Siliconized Low-Retention Microcentrifuge Tubes (Fisherbrand)	Fisher Scientific	Cat.# 2.0MLGRD FLTP LW RT
Di(N-succinimidyl) glutarate (DSG) ≥ 97.0% (CHN)	Sigma-Aldrich	Cat.# 80424
Formaldehyde Solution, 16%,	Fisher Scientific Uk Ltd	Cat.# 10751395
GeneJET PCR Purification Kit	ThermoFisher Scientific	Cat.# K0701
Dynabeads Protein G for Immunoprecipitation	ThermoFisher Scientific	Cat.# 10003D
2′-deoxycytidine	Berry & Associates	Cat.# PY 7216
2′-deoxyguanosine	Berry & Associates	Cat.# PR 3452
C5-hydroxymethyl-2′-deoxycytidine	Berry & Associates	Cat.# PR 7588
C5-methyl-2′-deoxycytidine (5-mC)	Carbosynth	Cat.# ND06242
QuickExtract DNA Extraction solution	Epicenter	Cat.# QE09050
MyTaq Red DNA Polymerase	Bioline	Cat.# BIO-211XX
Amyloid β-Protein (1-42) (HFIP-treated)	Bachem	Cat.# 4090148.XXXX
Bovine serum albumin (BSA)	Sigma-Aldrich	Cat.# A2153
Critical Commercial Assays		
Dynabeads mRNA DIRECT Purification Kit	ThermoFisher Scientific	Cat.# 61011
ScriptSeq Complete Gold Kit	Epicenter	Cat. # BEP1224
EpiTect Bisulfite Kits	QIAGEN	Cat. # 59104
eBioscience Annexin V-FITC Apoptosis Detection Kit	ThermoFisher Scientific	Cat.# BMS500FI-XXX
CellTiter-Glo® Luminescent Cell Viability Assay	Promega	Cat.# G7570
Deposited Data		
Murine BV2 RNA seq data (Raw data)	This paper	GEO: GSE105155
Experimental Models: Cell Lines		
Mouse: BV2. Passage ≤ 25 (Female)	Bertrand Joseph's lab (Shen et al., 2016)	RRID:CVCL_0182
Human: CHME3 (also known as HMC3). Passage ≤ 25 (Undetermined sex)	ATCC	ATCC® CRL-3304; RRID:CVCL_II76
Experimental Models: Organisms/Strains		
Mouse: 5xFAD: B6. SJL-Tg(APPSwFlLon, PSEN1*M146L*L286V)6799Vas/Mmjax) (Male)	The Jackson Laboratory	Cat.# 34840-JAX
Mouse: TET2$^{floxed/floxed}$: B6;129STet2tm1.1Iaai/J (Male)	The Jackson Laboratory	Cat.# 017573
Mouse: CX3CR1$^{CreERT2/WT}$: B6.129P2(Cg) Cx3cr1tm2.1(cre/ERT)Litt/WganJ (Male)	The Jackson Laboratory	Cat.# 021160
Rat: Wistar IGS (Male)	Charles River	Cat.# Crl:WI
Mouse: CD-1® IGS (Male)	Charles River	Cat.# Crl:CD1(ICR)
Oligonucleotides		
See Table S1 (For primer list for RT-qPCR)	This paper	N/A
See Table S2 (For primer list for ChIP)	This paper	N/A
See Table S3 (For primers list for Ox-Bs sequencing)	This paper	N/A
siGENOME Non-Targeting siRNA #2	Dharmacon	Cat.# D-001210-02-xx
Silencer® Select Pre-Designed siRNA-Tet2	Life Technologies	Cat.# S103016
Flox Tet2 (Forward primer for genotyping) AAGAATTGCTACAGGCCTGC	This paper	Sequence obtained from (Moran-Crusio et al., 2011)

(*Continued on next page*)

Continued		
REAGENT or RESOURCE	SOURCE	IDENTIFIER
Flox Tet2 (Reverse primer for genotyping) TTCTTTAGCCCTTGCTGAGC	This paper	Sequence obtained from (Moran-Crusio et al., 2011)
Deleted TET2 (LoxP3R for genotyping) TAGAGGGAGGGGGCATAAGT	This paper	Sequence obtained from (Moran-Crusio et al., 2011)
Software and Algorithms		
Statgraphics Centurion XVII	Statgraphics	RRID:SCR_015248
Trim Galore	https://www.bioinformatics.babraham.ac.uk/projects/trim_galore/	RRID:SCR_011847
Bismark	https://www.bioinformatics.babraham.ac.uk/projects/bismark/	RRID:SCR_005604
Tophat	https://ccb.jhu.edu/software/tophat/index.shtml	RRID:SCR_013035
Seqmonk	https://www.bioinformatics.babraham.ac.uk/projects/seqmonk/	RRID:SCR_001913
DESeq2	https://bioconductor.org/packages/release/bioc/html/DESeq2.html	RRID:SCR_016533
topGO	http://bioconductor.org/packages/release/bioc/html/topGO.html	RRID:SCR_014798
Fiji ImageJ	http://fiji.sc/	RRID:SCR_002285
GraphPad Prism 7	https://www.graphpad.com/scientific-software/prism/	RRID:SCR_002798
ZEN Zeiss software (version 14.0.18.201)	https://www.zeiss.com/microscopy/us/products/microscope-software/zen.html#introduction	RRID:SCR_013672

LEAD CONTACT AND MATERIALS AVAILABILITY

This study did not generate new unique reagents. Further information and requests for resources and reagents should be directed to and will be fulfilled by the Lead Contact, Miguel Angel Burguillos (maburguillos@us.es).

EXPERIMENTAL MODEL AND SUBJECT DETAILS

Cell Lines and siRNA Transfection

Human CHME3 (undetermined sex) and murine microglial BV2 (female) cell line were cultured as described in Shen et al. (2016). Briefly, the cells were maintained in 10% fetal calf serum (FCS) in DMEM and reduced to 5% FCS during the experiments supplemented with penicillin/streptomycin (100 U/ml and 100 μg/ml respectively). Transfection of BV2 cells was carried out using Lipofectamine 3000 (Invitrogen) following the manufacturer's instructions.

Animals and Subject tissue

18-month-old male B6. SJL-Tg (APPSwFlLon, PSEN1*M146L*L286V)6799Vas/Mmjax), called 5xFAD (generously provided by Dr. Javier Vitorica) and 8 to 12-week-old male B6;129STet2tm1.1Iaai/J, called $TET2^{floxed/floxed}$, B6.129P2(Cg) Cx3cr1tm2.1(cre/ERT) Litt/WganJ, called $CX3CR1^{CreERT2/WT}$ (both Jackson Laboratories), and CD-1® IGS mice and Wistar IGS rats (both Charles River) were kept under controlled light (12-hr light/dark cycles) and temperature (22°C-24°C) and with free access of food and water. For the generation of primary microglia cultures, both male and female pups were used.

For the LPS intraperitoneal experiment in mice, we followed the procedure detailed in Bodea et al. (2014). Briefly, injections in $Tet2^{flox/flox}Cx3cr1^{Cre/WT}$ and $Tet2^{flox/flox}Cx3cr1^{WT/WT}$ mice consisted in four daily injections with 1 μg per g of body mass per day of LPS or vehicle (PBS), and the analysis was performed on the fifth day since the start of the treatment (LPS *in vivo* experiments were carried out with LPS from Salmonella abortus equi while for the *in vitro* experiments, we used LPS from *Escherichia coli*, serotype 026:B6).

All experiments conducted with animals were previously approved by the different Ethical Committee for Experimental Research from University of Seville and University of Cambridge and fulfilled the requirements for experimental animal research in accordance with in accordance with the UK Animals (Scientific Procedures) Act (1986) and the Guidelines of the European Union Council (86/609/EU) and the Spanish and UK regulations (BOE 34/11370–421, 2013) for the use of laboratory animals.

Human brain tissue was obtained from 1 male (subject 3) and 2 females (subject 1 and 2) subjects who suffered and died from AD. The region investigated was the Temporal lobe. All sections were stained with hematoxylin and eosin and with antibodies against TET2, Iba-1 and Aβ. They were microscopically reviewed for verification of pathology. Before the investigation, the entire collection of brain sections, were subjected to a neuropathological whole-brain analysis for clinical diagnostic purposes, according to routine procedures at the University Hospital Virgen del Rocio, Seville (Spain). The project procedures involving human brain tissue was approved by the Regional Ethical Review Board, reference number C.P. 33170015 - C.I. 0422-N-17.

METHOD DETAILS

Generation of microglia Tet2-deficient mice

Tet2$^{flox/flox}$ C57BL/6 mice with the *Tet2* allele floxed at exon 3 (Jackson Laboratories, B6;129S-Tet2tm1.1Iaai/J) and C57BL/6 mice containing a Cre recombinase under the control of *Cx3cr1* promoter and enhancer elements (Jackson Laboratories, B6.129P2(Cg)-Cx3cr1tm2.1(cre/ERT)Litt/WganJ), were crossed to generate *Tet2*$^{flox/flox}$;*Cx3Cr1*$^{Cre/WT}$ (experimental mice) and *Tet2*$^{flox/flox}$;*Cx3Cr1*$^{WT/WT}$ (control mice).

The genotype of *Tet2*$^{flox/flox}$; *Cx3Cr1*$^{WT/WT}$ and *Tet2*$^{flox/flox}$;*Cx3Cr1*$^{Cre/WT}$ mice was determined by analysis of DNA extracted from the fingers using a QuickExtract (Epicenter) and amplified with MyTaq Red DNA Polymerase (Bioline). The deletion of the *Tet2* gene was determined by analysis of DNA extracted from isolated primary microglia using a QuickExtract DNA Extraction solution (Epicenter) and amplified with MyTaq Red DNA Polymerase (Bioline).

The PCR consisted of 94°C for 1min, then 35 cycles with denaturation at 95°C for 15 s, annealing at 58°C for 15 s, and elongation at 72°C for 10 s. The primer sequences used were obtained from a previous study (Moran-Crusio et al., 2011).

Primary microglia cell culture preparations

Rat glial cultures were prepared from postnatal day 5-7 rat cerebral hemispheres as described previously (Bal-Price and Brown, 2001). Cortical hemispheres were dissected and meninges, blood vessels as well as white matter were removed. Tissue was transferred to pre-warmed HBSS containing 0.17% trypsin (37°C), chopped thoroughly and incubated for 15-20 min.s at 37°C, 5% CO_2. Supernatant was removed and remaining trypsin was neutralized by addition of an equal amount of deoxyribonuclease I solution (0.02 mg/ml) in glial culture medium: DMEM supplemented with 10% FCS and antibiotics gentamicin (50 μg/ml) or penicillin/streptomycin (100 U/ml and 100 μg/ml respectively). Tissue was mechanically dissociated by repeated trituration through fire-polished glass Pasteur pipettes of two decreasing aperture sizes; and the suspension was centrifuged at 150 × g for 7 min.s at room temperature (RT). The pellet was resuspended in glial culture medium, and this suspension was sequentially passed through a 100 μm and 40 μm cell-strainers (BD Biosciences). Cells were plated at a density of 10^5 cells/cm^2 onto 24-well plates or into T75 cell culture flasks (Nunc) that were coated with poly-L-lysine (0.0005% in PBS) for at least 30 min at RT. After 24 h plates or flasks were carefully tapped to dislodge sedimentary cell debris, and medium was exchanged. Cultures were maintained at 37°C in a humidified atmosphere of 5% CO_2/ 95% O_2. Cells were stimulated after 7-9 days *in vitro* (DIV). Pure microglial cultures were obtained from mixed glial cultures (7-9 DIV). Culture flasks were gently vortexed for ~1 min., supernatant containing detached microglial cells was collected and centrifuged at 150 × g for 7 min at RT. Microglia cells were resuspended in conditioned glial medium mixed with fresh glial medium (at the ratio 2:1) and plated at a density of 2.5-5 × 10^4 cells/cm^2 onto 6- or 24-well plates (Nunc) coated with 0.0005% poly-L-lysine.

Primary adult murine microglia cultures from 10-12-week old adult mouse cortices were carried out as previously described (Yip et al., 2009). Briefly, adult CD1 male mice were deeply anaesthetized with sodium pentobarbital, then perfused with saline to remove peripheral monocytes/macrophages. The cortical region was dissected out and placed into ice-cold Hanks Balanced Salt Solution (HBSS) media. The meninges were removed prior cutting into longitudinally segments using a tissue chopper. After digestion in papain followed by dissociation, the cell suspension was passed through a 70 μm sieve. The cells were plated into each well containing an ethanol-cleaned coverslip. After 2 h, unattached cells were washed away with DFP media (containing Dulbecco's modified eagle medium (DMEM)), 15% heat-inactivated fetal bovine serum (HI-FBS) and penicillin-streptomycin; 100 IU/ml), and allowed to incubate overnight at 37°C and 5% CO_2 and were used the next following day for experimental studies.

Primary postnatal mouse microglial cells were prepared from P1-4 experimental and control mouse brain following described protocol (Deierborg, 2013). Postnatal P1-4 mice were decapitated and brains were carefully dissected removing all the meninges and the cortices were washed in ice-cold Ca^{2+}- and Mg^{2+}-free Hanks' buffered salt solution (HBSS; Biowest). Later on, they were minced, and resuspended in ice-cold HBSS. After being washed, tissues were incubated for 15 min in HBSS containing 0.1% trypsin and DNase 0.05%, and resuspended in DMEM medium containing 10% FBS and 1% P/S (DMEM high glucose, Biowest). Cells were cultivated in a T25 flask. Medium was replaced completely after 1 day seeding and 7 days after seeding.

Deletion was induced upon 4-OH-tamoxifen treatment for 48 h before harvesting of microglia. Microglial cells were harvested from confluent astrocyte monolayers, 14 days after the initial seeding, by tapping the side of the culture flask. These microglial cells found in the medium were plated into 12-well dishes. Experiments were performed 24 h after the final plating.

We regularly tested the purity of our primary microglia cell cultures and observed consistently that over 80% of our cultures were positive to Iba-1 staining, and therefore microglia cells.

RT-qPCR analysis

Total RNA was extracted using the TRIzol reagent (Sigma Aldrich) following the manufacturer's instructions. Using the RevertAid First Strand cDNA Synthesis Kit (Thermo Scientific, UK), 1 μg of the total RNA was transformed into cDNA. qPCR was performed using the MESA BLUE SYBR® Assay (Eurogentec, UK). Results were calculated using delta Ct method and represented as absolute values with arbitrary units. *Atp5b* and *Actb* genes were used as housekeeping genes in murine samples, *Actb* was used as a housekeeping gene in rat samples and PGK1 was used as housekeeping gene in human samples.

Immunofluorescence for mouse material

5xFAD mice (18 months old; kindly provided by Dr. Javier Vitorica), a model for Alzheimer disease and LPS intraperitoneally injected mice, were transcardially perfused under deep anesthesia with 4% paraformaldehyde and PBS, pH 7.4. Brains were removed, cryoprotected in sucrose and frozen in isopentane at −15°C and serial coronal sections (30 μm thick) were cut with a cryostat, and further processed. Briefly, the tissue was subjected to antigen retrieval (10mM citrate buffer pH 6.0. 80°C in a water bath for 30 min). Later on, the brain sections were permeabilized with 1% (v/v) Triton X-100 in PBS for 1 h, and then incubated in 5% (w/v) BSA, 1% Triton X-100 in PBS for 1 h, to prevent unspecific staining. The tissue was then incubated overnight at 4°C with the primary antibodies against Aβ (1:1000, Sigma-Aldrich), Tet2 (1:250, Abcam), Iba 1 (1:500, Wako) and Cox-2 (1:100 R&D System) and the following day, the brain section was rinsed for 1 h in PBS containing 0.1% Triton X-100. After incubating for 1 h with the corresponding secondary antibodies (1:500; Alexa antibodies, Invitrogen), and rinsed again with PBS containing 0.1% Triton X-100 for 60 min. For staining with Hoechst (1μg/ml; Sigma Aldrich) sections were first washed in PBS containing 0.1% Triton X-100 and then incubated for 5 min. Next, we washed sections 2x10 min in in PBS containing 0.1% Triton X-100. The brain sections were mounted in Glycerol 50% for visualization in an inverted ZEISS LSM 7 DUO confocal laser-scanning microscope using a 63x oil objective with a numerical aperture of 1.3. Images from all experimental groups were obtained at the same day and under equal conditions (laser intensities and photomultiplier voltages).

Immunofluorescence for the subject material

Brain tissue sections were deparaffinized in xylene (15 min each) followed by two 10-min washes with ethanol 100%, two 10 min washes with ethanol 95% and three 5-min washes with distilled water. Tissue was subjected to heat-induced antigen retrieval with DAKO solution (pH 6.0; DAKO #S1699) for 40 min using a steamer. Subsequently, the tissue was left in the same solution until it reached room temperature. Next, three 10 min washes with TBS, followed by a 10 min TBS-Triton X-100 0.1% (v/v) and a final 10 min TBS were performed. The tissue was immersed in blocking solution (5% donkey serum in TBS-T 0.1%) for 1 h at room temperature). The antibodies were diluted in blocking solution overnight at 4C. The next day the slides were washed 5 times in TBS, incubated 1 h with the corresponding secondary antibodies, followed by five 10 min TBS washes. Finally, the tissue was processed following manufacturer's recommendation with Autofluorescence Eliminator Reagent (Millipore Catalogue number 2160) and mounted with Mount slides in Fluoromount-G (AH Diagnostics #0100-01) for confocal microscopy analysis. Images were acquired by Zeiss LSM700 confocal laser scanning microscope equipped with ZEN Zeiss software (version 14.0.18.201) and processed with Photoshop CC 2017.

Fluorescent intensity (CTCF) of Tet2 staining was measured using Fiji ImageJ, as described previously (McCloy et al., 2014) with modifications. In more details, single in-focus planes were captured using x 40 objective. Tet2 staining was converted to grayscale using Photoshop. Using ImageJ, an outline was drawn around the soma of each microglia and values including area and mean intensity were measured, along with 4 background readings from the same field of view. The corrected total cellular fluorescence (CTCF) = Integrated Density – (Area of selected cell (x) Mean fluorescence of background readings). At least 5 different plaques and at least 26 microglia from these plaques or 5 white matter single planes and at least 24 microglia per subject were scored for intensity. All microglia found in the plaques or in the white matter plane were scored. Areas where chosen based on Aβ staining in random. Analysis and plot was performed using GraphPad Prism 7.

RNA-seq

mRNA-seq libraries were prepared from 1 μg of total RNA using the Dynabeads mRNA purification kit (ThermoFisher Scientific) and the low input ScriptSeq Complete Gold Kit (Epicenter). Libraries were sequenced on an Illumina NextSeq 500 with single-end 75 bp reads. Reads were trimmed using Trim_galore! v0.3.3 and mapped using Tophat v2.0.9 (Trapnell et al., 2009) to the mm9 genome assembly. Raw read counts for each gene were generated in Seqmonk with the RNA-seq quantitation pipeline. DESeq2 was then used for differential expression analysis and for generating normalized gene expression values. Gene ontology analysis was performed using the R package topGO.

OxBS-seq

Deep sequencing of PCR products from BS- and oxBS-converted DNA was performed as previously described (de la Rica et al., 2016). Briefly, precipitated DNA (without glycogen) was resuspended in water and further purified using Micro Bio-Spin columns (Bio-Rad), after which half of the DNA was oxidised with 15 mM KRuO4 (Alfa Aesar) in 0.5 M NaOH for 1 h. Following bisulfite conversion of both DNA fractions with the EpiTect Bisulfite kit (QIAGEN), a two-step PCR amplification was used: a first PCR amplifies the region of interest and adds part of the sequencing adaptors; a second PCR on pooled amplicons then completes the adaptors and adds sample barcodes, allowing for multiplexing. Paired-end sequencing of pooled samples was done using an Illumina MiSeq. Data were aligned using Bismark (Krueger and Andrews, 2011) to a custom genome containing the amplicon sequences; only CpGs covered by at least 100 reads were used to calculate 5mC/5hmC levels.

Measurements of OCR and ECAR

Real-time measurements of oxygen consumption rates (OCR) and extracellular acidification rates (ECAR) were performed on a Seahorse XF-24 extracellular flux Analyzer (Seahorse Biosciences) according to manufacturer's instructions and as previously described (Volobоueva et al., 2013). BV2 treated cells were detached with the pipette after treatment and re-seeded 30,000 cells/well to precoated Seahorse XF-24 plates, are for metabolic analysis. The XF24 cell culture microplate was coated with BD Cell-Tak (BD Biosciences, cat# 354240). The day before the metabolic assay, 1 mL of Seahorse Bioscience XF Calibrant (pH 7.4) was added to each well of the XF-24 utility plate, position the sensor cartridge on top of the utility plate, and incubated at 37°C overnight. BD Cell-Tak solution was prepared by adding 73 μL of 1.5 mg/ml stock concentration BD Cell-Tak to 1.1 mL sterile H_2O into a final concentration of 0.1 mg/ml. After that, 20 μL of the VD Cell-Tak solution was added to each well of a XF-24 cell culture plate, followed by 40 μL of 0.1M $NaHCO_3$ (pH 8.0) to each well to neutralize and promote BD Cell-Tak adsorption to the microplate. The microplate was incubated at 37°C minimum for 1 hour. Seahorse XF assay media (supplemented with 25 mM glucose, 2 mM glutamine and 1 mM sodium pyruvate) was prewarmed to 37°C prior to use. After cell count, cells were centrifuged at 300 g for 5 min and resuspend in the supplemented XF assay media at 3000 cells/ml. Each well of the Cell-Tak coated XF-24 cell culture microplate was washed with 200 μL of sterile water and 100 μL of cell suspension added, followed by centrifugation of the microplate at 700 g for 5 min to facilitate cell attachment. Cells were incubated at 37°C for at least 1 h to allow cell attachment. The different drugs were added automatically during measurement, after establishing baseline of oxygen consumption rates. We measured the OCR and ECAR in response to sequential treatment with the ATPase inhibitor oligomycin (2.5 μM), the uncoupling agent FCCP (1 μM) and the electron-transport-chain inhibitors rotenone (2 μM) and Antimycin A (1 μM).

Measurement of extra-cellular glucose

Glucose measurement was determined in the Department of Clinical Biochemistry, Royal London Hospital, UK. Briefly, medium from BV2 siControl and siTET2 cells alone or after LPS treatment was centrifuged and the supernatant was analyzed using the Accutrend®Plus System (Roche) according to the manufacturer's instructions.

Preparation of α-synuclein and Aβ-oligomers

For the preparation of α-synuclein fibrils, α-synuclein monomers were purchased from (Alexo Tech AB, Sweden). Briefly, a stock solution of α-synuclein (140 μM final concentration) was incubated for 6 days at 37°C, under continuous agitation as described previously in Hornedo-Ortega et al. (2016). For the preparation of Aβ oligomers, 1mg of HFIP-Aβ 1-42 (Bachem, H7442.1000) was carefully mix through pipetting in 200 μL of DMSO. Later on, 9800 μL of PBS was added to get a final concentration of 22 μM and it was aliquoted *in silico*nized Low-Retention Microcentrifuge Tubes (Fisherbrand™) and incubated at 37°C for 3h. After that aliquots were kept frozen at −80°C. Cells were incubated in the presence of α-synuclein fibrils and Aβ-oligomers to a final concentration of 5μM and 2μM respectively.

Immunoblotting

All cell extracts were processed for immunoblotting with a SDS-polyacrylamide gel electrophoresis as described previously (Burguillos et al., 2015). Briefly, Laemmli's loading buffer (100 μl/10^6 cells) was added to harvested cells and samples were boiled for 3 min. Thirty μl of protein extracts were resolved on 8, 0r 12% SDS polyacrylamide gel at 150 V and transblotted onto nitrocellulose membranes (0.2 μm) for 2 h at 200 mA. Membranes were blocked overnight in a buffer (50 mM Tris, pH 7.5, 500 mM NaCl) supplemented by 5% non-fat milk powder and probed with primary antibody for overnight, in blocking solution with 1% Bovine serum albumin, followed by the incubation with secondary antibody for 1 h at room temperature. After repeated washing in PBS bands were visualized by ECL according to the manufacturer's instruction. A complete list of primary antibodies can be found in the Key resources table. β-actin antibody (Sigma-Aldrich) was used to verify equal loading of the gel. Secondary horseradish peroxidase-conjugated anti-rabbit and anti-mouse antibodies were obtained from Dako.

Microglia cell counting

BV2 cell number quantification was performed using a NucleoCounter® NC-100 (Chemometec) according to manufacturer's instructions.

Apoptosis determination

Apoptosis was quantified using the Annexin V-FITC Determination Kit (eBioscience) according to the manufacturer's instructions. Briefly, cells medium and the cells were collect in a FACS tube. Annexin V-FITC (25 μg/ml) was added to the cell suspension. The cells were incubated for 10 min in darkness at RT. 1 μg/ml propidium iodide staining solution was then added and FACS was carried out using a BD FACS CANTO II flow cytometer.

Cell viability

Cell viability was quantified by CellTiter-Glo® Luminescent Cell Viability Assay according to the manufacturer's instructions. Detection is based on using the luciferase reaction to measure the amount of ATP from viable cells. The plate used was opaque to limit interference from external light. The intensity of the emitted light due to the degradation of D-Luciferin and ATP by the enzyme Luciferase is proportional to the amount of free ATP present at that moment in the cells.

Chromatin Immunoprecipitation

BV2 cells were treated with 1mg/ml of LPS during 6h. For each histone modification ChIP, the cells were washed with PBS and fixed by 1% formaldehyde for 12 min at RT. For NF-κB ChIP, the cells were first fixed with 2 mM DSG in PBS for 45 min at RT followed by 1% of formaldehyde fixation for 12 min. After stopping the fixation with 0.125 M glycine, the cells were washed with cold PBS and collected by centrifugation. Subsequently, the cells were washed with wash buffer (10 mM HEPES/KOH at pH 7.9, 85 mM KCl, 1mM EDTA, 0.5% IGEPAL) once, lysed with lysis buffer (50 mM Tris at pH 7.4, 1% SDS, 0.5% Empigen, 10 mM EDTA, 1mM PMSF) supplemented by protease inhibitors for 30 min on ice and the chromatin was sonicated to an average size of 300-700 bp. For immunoprecipitation, the soluble chromatin was diluted ten times in dilution buffer (50 mM Tris at pH 8.0, 0.5% NP-40, 0.2 M NaCl and 0.5 mM EDTA) and incubated with 5 μg of antibodies selective for NF-κB p65, H3K27ac, H3K4me1 or TET2 overnight at 4°C. The immune complexes were collected with protein G beads for 2 h at 4°C, washed with low salt buffer (50 mM Tris at pH 8.0, 0.1% SDS, 1% NP-40, 2 mM EDTA, 0.5% Deoxycholate and 0.15 M NaCl), high salt buffer (50 mM Tris at pH 8.0, 0.1% SDS, 1% NP-40, 2 mM EDTA, 0.5% Deoxycholate and 0.5 M NaCl) and LiCl buffer (50 mM Tris at pH 8.0, 1% NP-40, 2 mM EDTA, 0.5% Deoxycholate and 0.25 M LiCl), respectively. Immunoprecipitates were eluted in 1% SDS and 0.1 M sodium bicarbonate and the crosslinks were reversed overnight. After proteinase K digestion, DNA was extracted using GeneJET PCR purification kit. Immunoprecipitated DNA was analyzed by real time PCR using specific primers

Liquid chromatography-mass spectrometry

2′-deoxycytidine (dC), 2′-deoxyguanosine (dG) and C5-hydroxymethyl-2′-deoxycytidine (5-hmC) were purchased from Berry & Associates; C5-methyl-2′-deoxycytidine (5-mC) was purchased from CarboSynth. Genomic DNA was digested to nucleosides for a minimum of 9 h at 37°C using a digestion enzymatic mix (kind gift from NEB). All samples and standard curve points were spiked with a constant amount of isotope-labeled synthetic nucleosides: 100 fmol of dC* (13C,15N-dC) and dG* (13C,15N-dG) purchased from Silantes, 5 fmol of 5-mC* (d3-5-mC) and 250 amol of 5-hmC* (d2,15N2-5-hmC) obtained from T. Carell (Center for Integrated Protein Science at the Department of Chemistry, Ludwig-Maximilians-Universität München, München, Germany). The nucleosides were separated on an Agilent RRHD Eclipse Plus C18 2.1 × 100 mm 1.8u column by using the HPLC 1290 system (Agilent) and analyzed using Agilent 6490 triple quadrupole mass spectrometer. To calculate the concentrations of individual nucleosides, standard curves representing the ratio of the peak response of known amounts of synthetic nucleosides and the peak response of the isotope-labeled nucleosides were generated and used to convert the peak-area values to corresponding concentrations. The threshold for peak detection is a signal-to-noise (calculated with a peak-to-peak method) above 10.

Microglia morphology

The proportion of the different microglial morphology was estimated according with the follow classification (see Figure 6, insets): (1) Quiescent microglia with small cell bodies, fine cytoplasmic ramifications, and low to moderate Iba1 expression; (2) microglia with early-stage activation characterized by increased ramification of cytoplasmic processes and cell size, and enhanced Iba1 labeling; (3) Microglia corresponding to next step of activation is characterized by further thickening of processes and retraction of the thinest ones, as well as increased cell body size and Iba1 expression; and finally, (3) amoeboid cells, showing complete retraction of cytoplasmic processes with maintained high levels of Iba1 expression.

Images quantification

The proportion of microglia in the SN in each LPS experiment experimental group was estimated using cell counter plugin included in Fiji ImageJ (W. Rasband, National Institutes of Health) software. In the SN of the different experimental groups we measured the mean intensity of the specific fluoresce markers (TET2 and COX-2), in Iba1 positive cells. To do that, we performed mask outlined of Iba1 area using exactly the same value of threshold in each image and then, we measured automatically the mean intensity inside of these areas using, again, the Fiji software.

QUANTIFICATION AND STATISTICAL ANALYSIS

The statistical details of experiments, including statistical tests used, number of experiments, and dispersion and precision measures, can be found in the figure legends. The differences between control and experimental groups were evaluated with either two-tailed Student's t test, one way or two-way ANOVA with different corrections depending on the experiment. We used Statgraphics Centurion XVII (64-bit) for PC (http://www.statgraphics.com/centurion-xvii) and R software for Mac (https://www.r-project.org/) for the statistical analyses. $p < 0.05$ was considered as statistically significant.

DATA AND SOFTWARE AVAILABILITY

The accession number for the RNA-seq data reported in this paper is NCBI GEO: GSE105155.